Coordination Chemistry Reviews 254 (2010) 77–102

Contents lists available at ScienceDirect

Coordination Chemistry Reviews

journal homepage: www.elsevier.com/locate/ccr

Review

Thienyl—Appended porphyrins: Synthesis, photophysical and electrochemical properties, and their applications

Nicola M. Boyle [a], Jonathan Rochford [b], Mary T. Pryce [a,*]

[a] School of Chemical Sciences, Dublin City University, Dublin 9, Ireland
[b] Chemistry Department, Brookhaven National Laboratory, Upton, NY 11973-5000, United States

Contents

ARTICLE INFO

Article history:
Received 30 March 2009
Accepted 1 September 2009
Available online 6 September 2009

Keywords:
Porphyrin
Thienyl
Photophysical
Electrochemical
Oligothiophene

ABSTRACT

This review focuses on the synthesis, photophysical and electrochemical properties of thienyl porphyrins where processes such as electron transfer, energy transfer and electropolymerisation are discussed. The purpose of this review is to examine the influence of the thienyl ring, whether it be directly connected (*via meso* and β positions) or indirectly connected (*via* a covalent linker or axial coordination) on the ground and excited state electronic properties of the porphyrin macrocycle. Additionally, the importance of the electronic properties of a bridging oligothiophene between the porphyrin and another centre in supramolecular systems is discussed. Also included are applications of thienyl porphyrins in such areas as catalysis, therapeutics, (opto)electronics and electron-transfer/light-harvesting systems.

1. Introduction

The diverse applications of porphyrins and their metallated analogues are derived from their stable and rigid structure, which possesses unique photophysical and electrochemical properties. At present porphyrin-based systems are widely studied because of their catalytic [1], therapeutic [2] and potential optoelectronic applications [3]. The reversibility of the redox chemistry shown by porphyrins, i.e. the stability of both their mono- and di-cationic derivatives, makes them particularly attractive for photoionisation and photoconductive processes. Such studies are well documented in the mimicking of the photosynthetic reaction centre by photoinduced electron transfer using porphyrin based electron reservoirs [4]. Extended π-conjugated porphyrin systems are increasingly investigated due to their applications towards advanced technologies, which include nonlinear optical materials [3]. The properties of the porphyrin macrocycle can easily be modulated by appending various chemical moieties onto the periphery of the ring, and

* Corresponding author. Tel.: +353 17008005; fax: +353 17005503.
E-mail address: mary.pryce@dcu.ie (M.T. Pryce).

0010-8545/$ – see front matter © 2009 Elsevier B.V. All rights reserved.
doi:10.1016/j.ccr.2009.09.001

also by varying the metal centre. Desirable molecular and material properties, such as large hyperpolarisabilities, can therefore be imparted on the porphyrin ring by appropriate substitution and metallation.

The covalent attachment of the thiophene ring to the porphyrin macrocycle is an attractive proposition as these compounds have independently been shown to have remarkable photophysical and electrochemical properties respectively. As literature reports of thienyl porphyrin systems are varied at best, with differing opinions on the influence of the thienyl ring on the macrocycle, an attempt is made here to correlate previous findings in a concise manner. Synthetic approaches towards various thienyl porphyrin structures are briefly described, and their photophysical properties discussed. Also, as the HOMO and LUMO energies are closely related to the standard reduction potentials, electrochemical properties of thienyl porphyrins are also incorporated where appropriate, thus providing an indication of the influence of the thienyl substituent on the magnitude of the porphyrin band gap—an important property when considering such complexes in supramolecular assemblies, photovoltaics or dye sensitised solar cell devices. There is an appreciable amount of literature on the synthesis and properties of pseudo-porphyrins and core modified porphyrins containing the thiophene ring, therefore the following discussion will deal only with porphyrins containing the traditional N_4-core, peripherally substituted with substituents incorporating the thiophene ring [5].

2. *Meso* and β-thienyl porphyrins

2.1. Synthesis

The first reported thienyl substituted porphyrin, *meso* tetra(thien-2-yl)porphyrin (**H_2P1**, Fig. 2) was synthesised by Triebs et al. in 1968 [6]. The direct condensation of pyrrole and 2-thiophenecarboxaldehyde *via* an adapted Rothemund method (route A, Fig. 1) resulted in the pure porphyrin in 9% yield. The Adler–Longo method was later applied by Torréns et

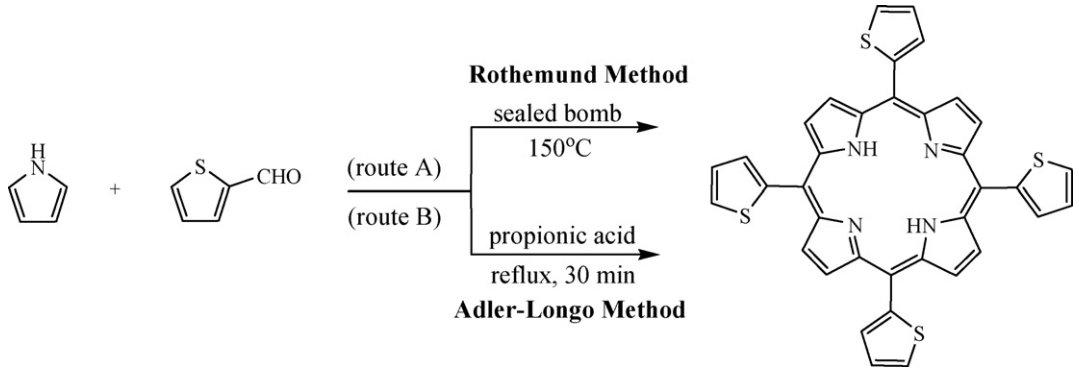

Fig. 1. Rothemund (route A) and Adler–Longo (route B) synthesis of *meso* tetra(thien-2-yl)porphyrin.

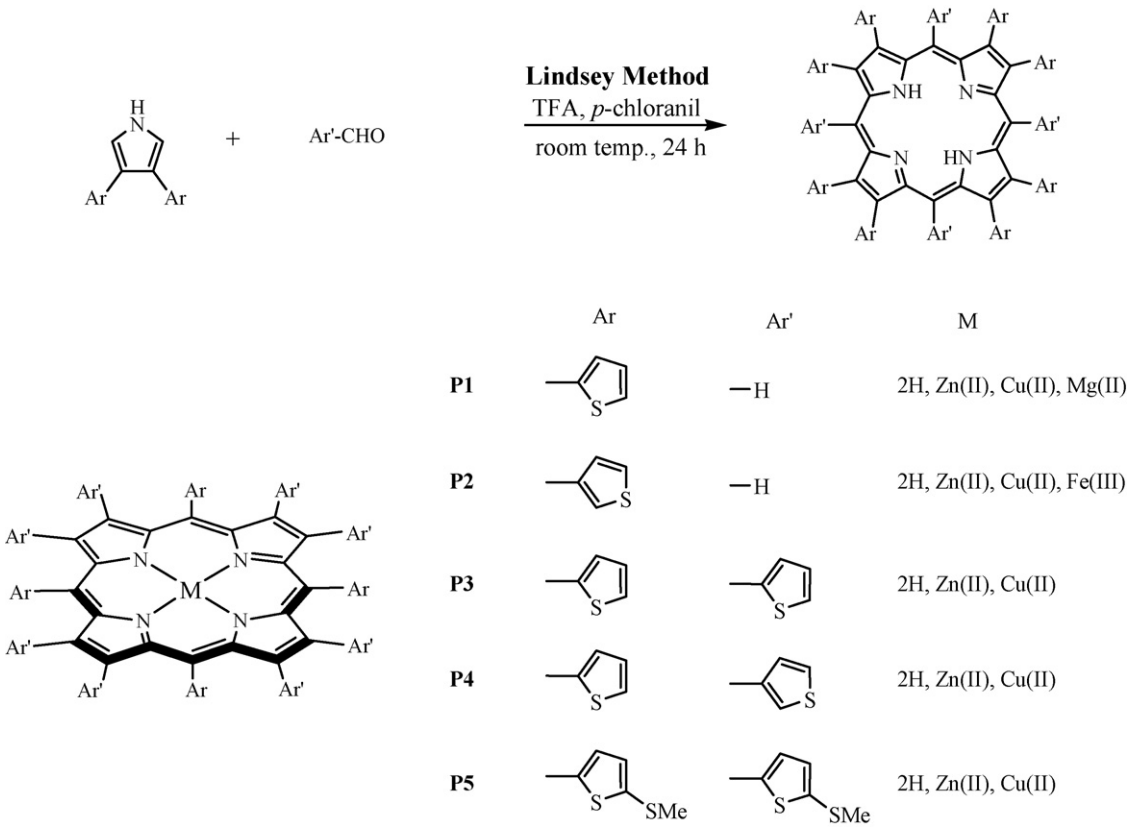

Fig. 2. Synthesis and structures of highly substituted thienyl porphyrins reported by Ono et al. [10].

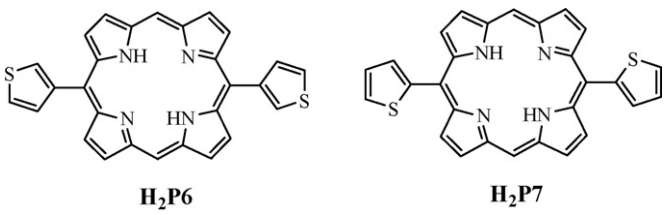

Fig. 3. 5,15-Bis(thienyl)porphyrins structural isomers prepared by the the Mac Donald 2 + 2 procedure [15,16].

al. however the yield was never reported (route B, Fig. 1) [7]. The *meso* tetra(thien-2-yl)porphyrin was prepared by reacting equi-molar amounts of 2-thiophenecarboxaldehyde and pyrrole in refluxing propionic acid, followed by recrystallisation. Both *meso* tetra(thien-2-yl)porphyrin and *meso* tetra(thien-3-yl)porphyrin (**H_2P2**, Fig. 2) were later reported by Bhyrappa and Bhavana using the Adler–Longo method to give the target compounds in 14% yield [8].

Ono et al. synthesised a series of *meso*- and β-dodecasubstituted thienyl porphyrins (**H_2P1**, **H_2P3**, **H_2P4**, **H_2P5**, Fig. 2) including the zinc and copper metallated derivatives by an adapted version of Lindsey's method [9] in an attempt to alter the redox potentials of the macrocyclic structure by inducing ruffling of the planar geometry into the macrocycle [10]. Using 3,4-diarylpyrroles and thienyl carboxaldehydes a series of highly substituted dodecathienyl porphyrins were produced under relatively mild conditions (Fig. 2).

The majority of studies to date have adapted the Lindsey procedure. This is advantageous due to its mild reaction conditions as opposed to the highly oxidising environment of the Rothemund and Adler–Longo methods which may be unsuitable for the thienyl substrates [11–14]. A number of alternative novel approaches have been reported however. The *trans* substituted porphyrin, 5,15-bis(thien-3-yl)porphyrin (**H_2P6**, Fig. 3) was prepared by Arminger and Lash using the Mac Donald 2 + 2 procedure, which involves the condensation of 3-formylthiophene with dipyrrylmethane [15]. The thien-2-yl isomer, 5,15-bis(thien-2-yl)porphyrin (**H_2P7**, Fig. 3) was later synthesised by a similar method [16].

An innovative approach towards porphyrin synthesis was reported by Bonar-Law, where a range of porphyrins were prepared in surfactant solution, involving multicomponent covalent assembly in a micellar environment [17]. The micelles display the ability to collect and concentrate species from aqueous solution and so promote porphyrinogen assembly by binding the product more tightly than the reactants. The initial steps of the reaction are: the concentration of the reactants in the micelle, their condensation into linear chains and their cyclisation into a porphyrinogen. Subsequently, the porphyrinogen is irreversibly oxidised to the porphyrin. Several aspects of this method were investigated including, the reaction time, reactant and surfactant concentration as well as the reversibility of the reaction. In this manner freebase *meso* tetra(thien-2-yl)porphyrin (**H_2P1**, Fig. 2) was produced, with an isolated yield of 24%, which is comparable to reported yields *via* the Lindsey procedure. This method also represents a substantial improvement from the earlier harsh conditions of Rothemund and Adler–Longo.

Most recently, a high yielding synthesis of *meso* substituted thienylporphyrins has been reported by Shi and Wheelhouse [18]. Using an adapted method of Lindsey and Woodford [19], commercially available porphine was initially converted to Mg(II)-porphine. Mg(II)-5,10,15,20-tetrakisbromoporphine was synthesised *via* bromination of the Mg(II)-porphine precursor. Using standard Suzuki conditions, the authors coupled aryl boronic acid groups to the porphyrin macrocycle and subsequently removed the magnesium ion to yield the desired free base porphyrins (Scheme 1). In this manner freebase *meso* tetra(thien-3-yl)porphyrin (**H_2P2**, Fig. 2) was produced in 41% total yield. However as this yield is based purely on functionalisation of the commercially sourced porphine it cannot be directly compared with former methods which involve the yield limiting porphyrinogen cyclisation step.

A few examples where further functionalisation of the thienylporphyrin have been reported utilising various C–C coupling reactions [20,21]. For example Rochford et al. reported a series of *meso* mono-, di-, tri- and tetra(thien-2-yl)porphyrins (**ZnP8**–**ZnP13**, Fig. 4) to investigate the influence of the thiophene ring on the ground and excited state properties of the porphyrin macrocycle [21]. The mono-, di- and tri- substituted porphyrins were prepared by a mixed aldehyde condensation of 5-bromo-2-thiophenecarboxaldehyde with benzaldehyde and pyrrole followed by metallation with zinc acetate and Sonogashira coupling with trimethylsilylacetylene.

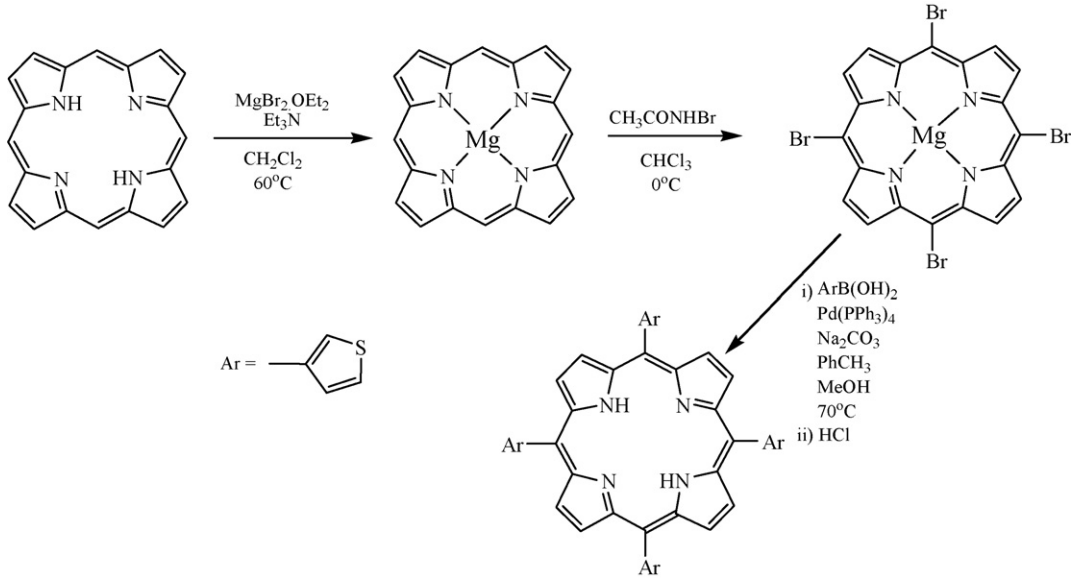

Scheme 1. Shi and Wheelhouse procedure [18].

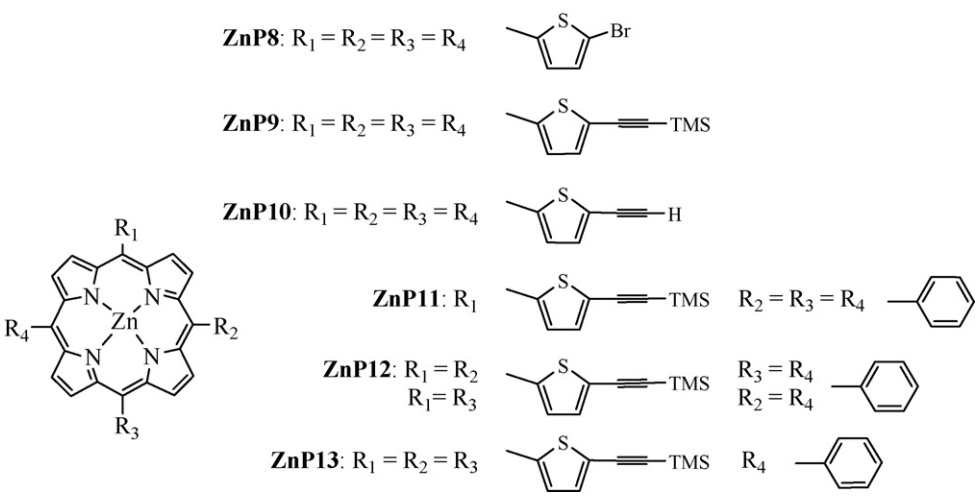

Fig. 4. Various thienyl porphyrins with extended conjugation [21].

Post functionalisation of the porphyrin ring is a method often used in the preparation of polymeric thienylporphyrin systems [22–24]. For example, two-dimensional porphyrin polymers containing oligothienyl bridges in the lateral direction were prepared (Fig. 16) by electrochemical oxidation of the zinc(II) and palladium(II) *meso* tetrakis(oligothienyl)porphyrin complexes (Fig. 5) [24].

Modern metal-catalysed bond-forming reactions were employed and facilitated the construction of **ZnP16**–**ZnP21** (Fig. 6) [25]. Combining electron-rich Suzuki-porphyrin synthon precursors, a variety of appropriately functionalised porphyrins were produced. These chromophores possess electron-poor thiophene and oligothiophene species linked by a direct carbon–carbon single bond or alternatively are covalently attached *via* an intervening ethynyl unit. Following this work, a series of conjugated zinc(II) porphyrin-based chromophores related to **ZnP19** were synthesised (**ZnP22**–**ZnP25**, Fig. 6) using similar metal catalysed cross-coupling reactions.

The crystal structure of **ZnP1** indicates that the porphyrin possesses a wave like conformation [26]. **CuP1** has a near planar porphyrin core with only slight puckering [27] with a deviation of less than 0.01 Å observed for individual atoms in the mean plane. In contrast **ZnP2** exhibits unusual planar and non-planar core features (Fig. 7) [28]. In the case of the planar core, only minimal deviation from planarity is observed with the β-pyrrolic carbons showing marginal deviation from the mean plane (±0.034 Å). The non-planar porphyrin showed core atoms displaced over the mean plane and geometry close to saddle-like conformation. In the case of the non-planar thienyl porphyrin the β-pyrrolic carbons show significant deviation (±0.422 Å). This deviation suggests the conformation is a combination of saddle and marginal ruffle. The crystal structure of 5,10,15,20-tetrakis(5′methylthien-2-yl)porphyrin, **H_2P26**, possesses an essentially planar geometry with a slight waving conformation [29]. A direct correlation between the degree of porphyrin distortion and the bathochromic shift in absorption spectra was shown for a series of β-, *meso*- overcrowded porphyrins [10].

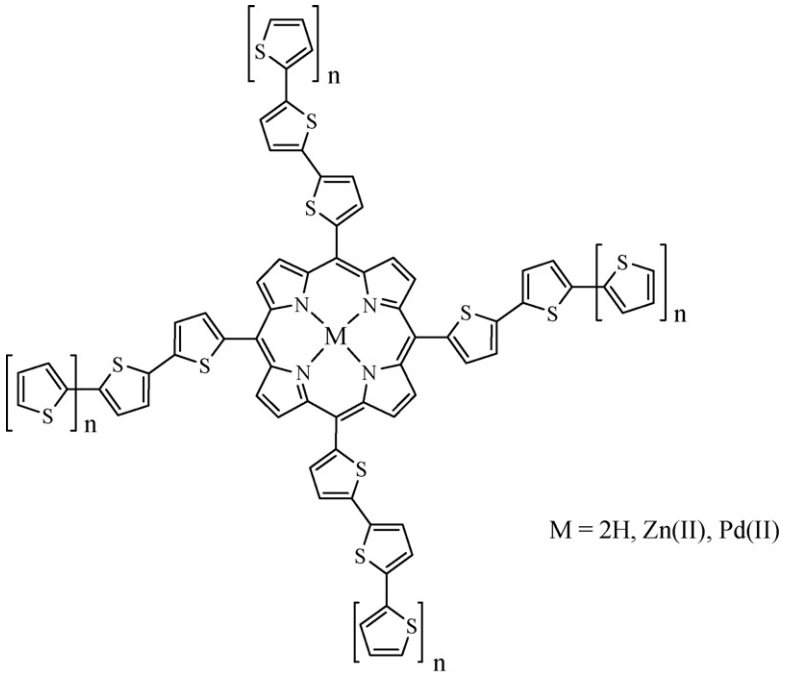

Fig. 5. P14: $n = 0$, **P15**: $n = 1$ [24].

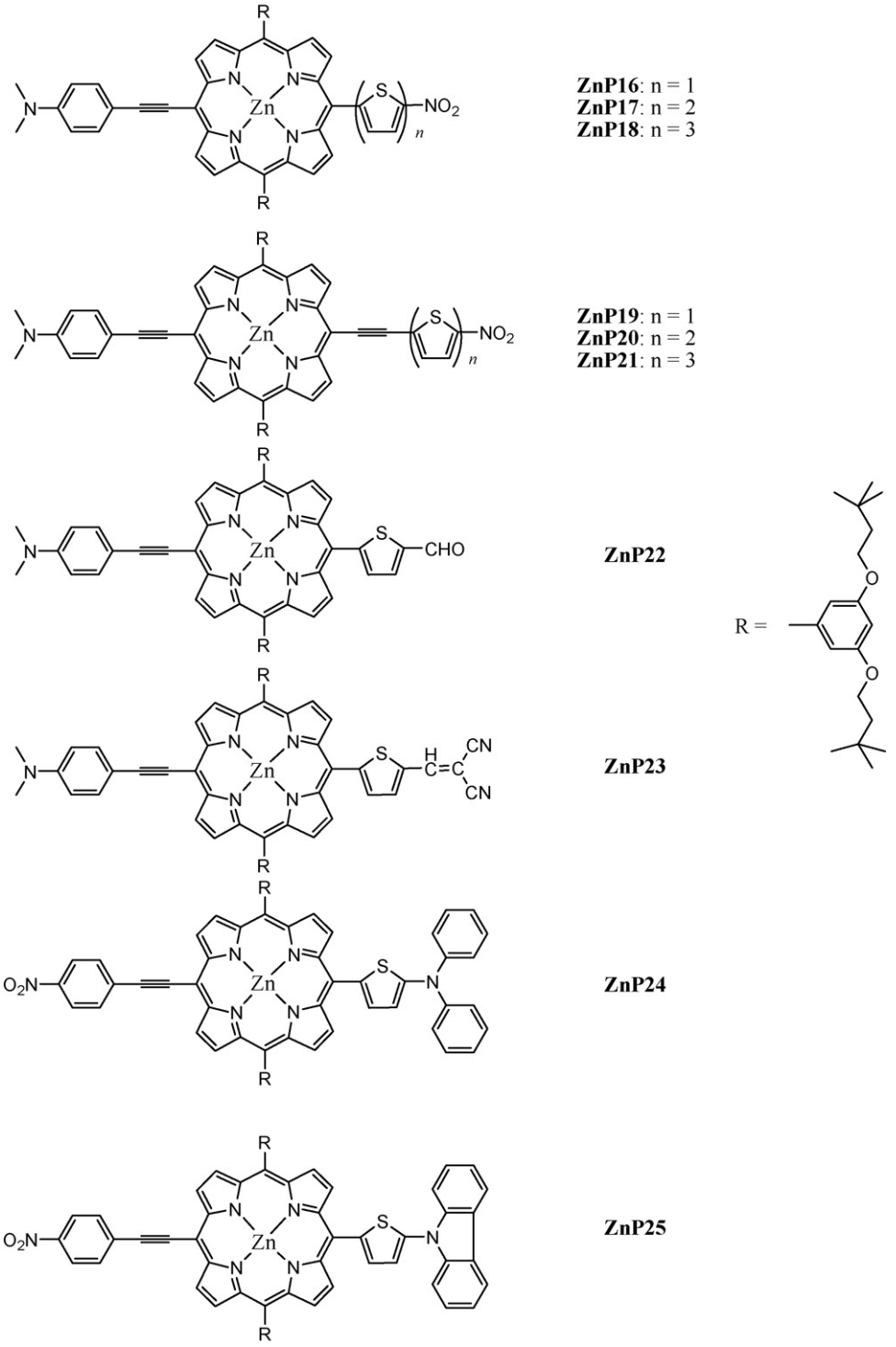

Fig. 6. ZnP16–ZnP25 [25].

For example **H_2P3** displays a remarkable bathochromic shift of *ca.* 4296 cm^{-1} of the Soret band relative to **ZnTPP**. Although the crystal structure of **H_2P3** has not been reported a saddle conformation was assumed based on reduced deshielding of its core N–H protons *via* ^{1}H NMR spectroscopy.

The macrocyclic core of the *trans* porphyrin **H_2P7** (Fig. 3) adopts a saddle like conformation in the solid state with the two *meso* thienyl arms parallel to each other [16]. These arms are tilted with respect to the porphyrin mean plane at angles of ~50° (smaller than that of **ZnP2**). In solid state packing, the thienyl groups form a staggered arrangement, with the aromatic core of the porphyrins forming a supramolecular columnar structure (Fig. 8).

2.2. Electronic and photophysical properties

Although the electronic and photophysical properties of thienyl porphyrins have been investigated by several groups there is little consistency in describing the influence of the thienyl ring on the electronic properties of the porphyrin molecule (e.g. inductive *vs.* electronic effects). The absorption spectrum of thienyl porphyrins

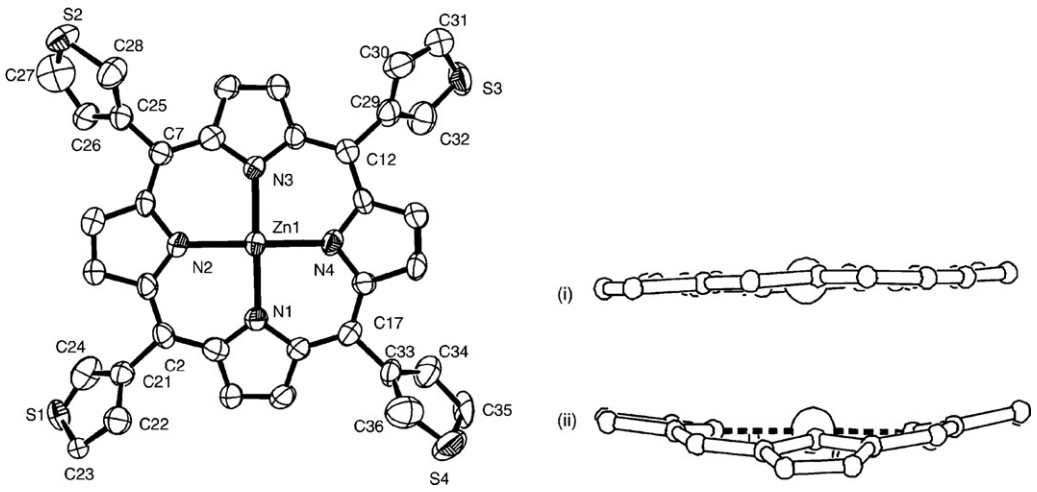

Fig. 7. Solid state crystal structure of the planar unit of **ZnP2**, (i) and (ii) indicate the side view of the planar and nonplanar porphyrin units respectively [28]. Reproduced from reference [28] with permission of the copyright holders.

has long been known to shift to longer wavelengths when compared to their tetraphenyl analogues (**H_2TPP**) (Table 1). Distortion of the planar macrocycle and the reduced dihedral angle of the thienyl group at the porphyrin ring result in an increase in conformational freedom for these systems with respect to **ZnTPP**, and also electronic consequences which are manifested in decreased Φ_{fl} and k_{fl} and increased k_{nr} [21].

The spectral profile of the zinc and copper metallo-derivatives (**ZnP1**, **ZnP2**, **CuP1**, **CuP2**, Fig. 2) reported by Bhyrappa and Bhavana are quite similar to those of the corresponding tetraphenylporphyrin analogues, each displaying an intense Soret and two Q bands [8]. Minor bathochromic shifts were observed for the zinc analogues (**ZnTPP**: 422 nm, **ZnP1**: 427 nm, **ZnP2**: 422 nm), as shown in Fig. 9 attributed to inductive effects, with greater shifts observed for the copper analogues (**CuTPP**: 415 nm, **CuP1**: 421 nm, **CuP2**: 418 nm). The molar extinction coefficients are comparable to tetraphenylporphyrins.

Table 1
Absorption and emission data of *meso* tetrathienylporphyrins and **H_2TPP** in CH_2Cl_2 [30,31].

Porphyrin	λ_{max} Soret (nm)	λ_{max} Q bands (nm)	λ_{em} (nm)	Stokes shift (cm^{-1})
H_2TPP	417	514, 549, 588, 647	651, 715	95
H_2P1	426	523, 558, 594, 661	670, 720 (sh)	204
H_2P2	421	519, 556, 594, 653	661, 723	185
H_2P8	425	521, 557, 596, 663	668	113
H_2P27	430	526, 569, 597, 665	674 (br)	201
H_2P28	425	520, 557, 597, 660	666, 725	136

In a similar study, Sun et al. reported the absorption λ_{max} and extinction coefficients of **H_2P1**, **H_2P8**, **H_2P27**, **H_2P28** and observed red shifts of between 238 and 725 cm^{-1} with respect to **H_2TPP**

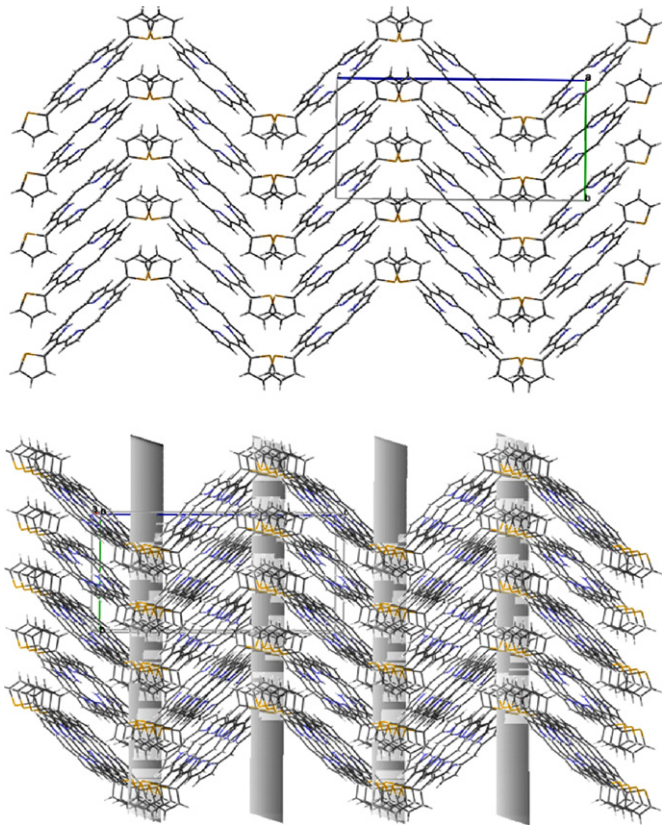

Fig. 8. Side view of stacking arrangement generated by **H_2P7** in the solid state [16]. Reproduced from reference [16] with permission of the copyright holders.

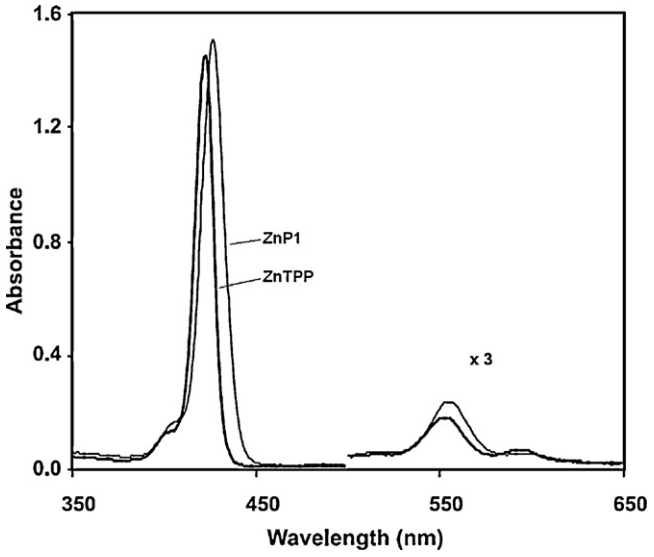

Fig. 9. Electronic absorption spectra of **ZnTPP** and **ZnP1** in CH_2Cl_2 [8]. Reproduced from reference [8] with permission of the copyright holders.

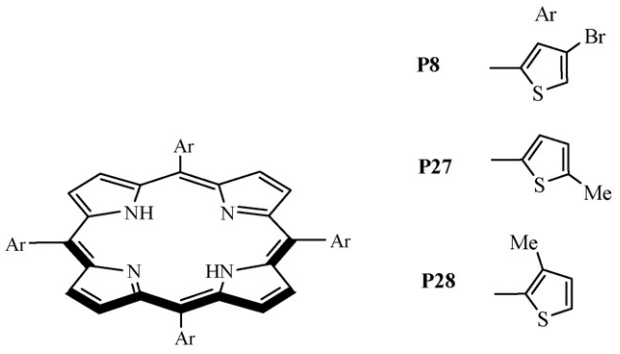

Fig. 10. Substituted *meso* thienyl porphyrins produced by Sun et al. [30].

[30]. The spectral shifts in the UV–vis spectra are attributed to the inductive effect of the thienyl group as opposed to the increased conjugation of the porphyrin π-system.

Recently, however, Brückner et al. investigated the electronic absorption properties of a number of related thienyl porphyrins (**H_2P1** and **H_2P2**, Fig. 2, **H_2P27** and **H_2P28**, Fig. 10) [31]. The Soret and Q bands of all the thienyl porphyrins are red shifted when compared to **H_2TPP** with its Soret band at 417 nm (Table 1). The Soret band of **H_2P2** was only slightly shifted to 421 nm. However the Soret bands of the methyl substituted thien-2-yl porphyrins are red shifted by some 452–725 cm^{-1} depending on the position of the methyl group. Such fundamental observations, although not conclusive, indicate a definite influence of the *meso*-thienyl substituents on the electronic properties of the central porphine ring. As part of the investigation into the origin of the bathochromic shifts in the absorption spectra of thienyl porphyrins, Brückner et al. employed density functional theory to compute the energy of the porphyrin system as a function of the rotation of a single *meso* aryl group. Reduced steric hindrance was found for the smaller five membered *meso* thienyl rings when compared to the larger six membered phenyl ring. In addition, the thien-2-yl group lacks one *o*-phenyl H to β-pyrrole H interaction (Fig. 11). This allows for greater ease of rotation of the thien-2-yl porphyrins and also a somewhat more facile rotation for the thien-3-yl porphyrins. The computed rotational barriers of **H_2P1** and **H_2P2** are 50 and 75% lower, respectively, compared to that of **H_2TPP**, thus allowing the thienyl groups to adopt a co-planar arrangement to the porphyrin ring.

This suggests that, the previous proposal, of bathochromic shifts observed in thienyl porphyrins, due to the thienyl rings inductive effect, is over simplified. The molecular modelling results indicate that these shifts may be more dependent on the conformation which the thienyl groups adopt allowing π–π orbital overlap of

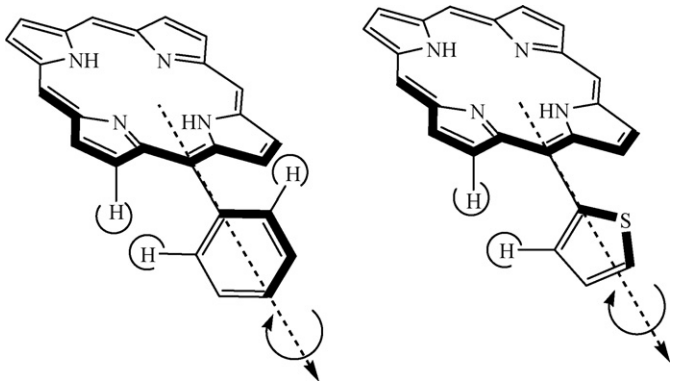

Fig. 11. Schematic of rotation for phenyl and thienyl *meso* substituent at the porphyrin ring [31].

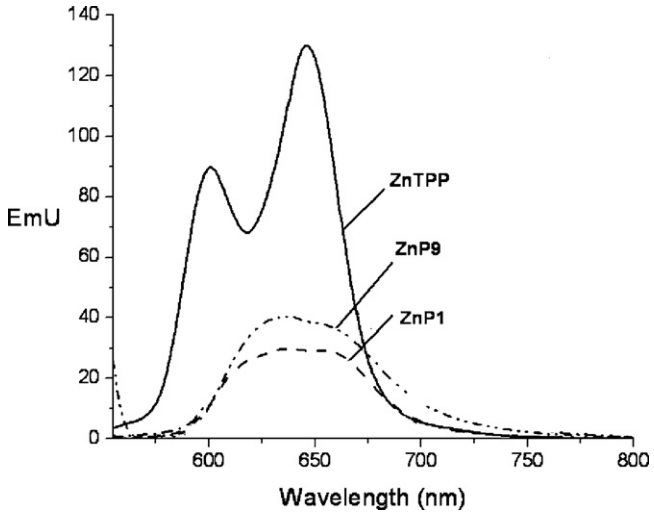

Fig. 12. Steady-state emission spectrum of **ZnTPP**, **ZnP1** and **ZnP9** (λ_{exc} = 550 nm, abs. = 0.2 at 550 nm), recorded in toluene at room temperature [32].

the thienyl and porphyrin ring systems as opposed to solely an inductive effect.

Remarkable bathochromic shifts of up to 4749 cm^{-1} for Soret bands were observed by Ono et al., thus confirming a direct correlation between the degree of porphyrin distortion and the bathochromic shift in absorption spectra for the overcrowded porphyrins **H_2P3**, **H_2P4** and **H_2P5** (Fig. 2) [10]. **H_2P3** and **H_2P5** have Soret bands with λ_{max} at 508 and 520 nm respectively. The Soret band of 2,3,5,7,8,10,12,13,15,17,18,20-dodecaphenyl porphyrin was observed at 466 nm, suggesting that along with the distortion of the macrocycle the electronic influence of the peripheral thienyl groups has a significant effect on the ground state electronic properties of these porphyrins.

A more recent study on porphyrins **ZnP8**–**ZnP13** (Fig. 4) suggests that the direct attachment of the aromatic thiophene ring at the *meso* position of the porphyrin ring leads to electronic interaction of the two π-systems which can be enhanced by appropriate substitution [21]. By varying the substituent on the thiophene ring a bathochromic shift can be observed in the Soret band of the porphyrin. Again, when compared to **ZnTPP** the Soret band of **ZnP1** is red shifted by 8 nm, to 430 nm, while the other tetra substituted porphyrins **ZnP8**, **ZnP9** and **ZnP10** are further red shifted by an additional 4 nm, 8 nm and 6 nm respectively. Such a strong shift would not be predicted on the basis of an inductive effect alone. More likely is the increased coupling of the overlapping π-systems of the porphyrin and thiophene rings as is evident in increasing FWHM of the porphyrin Soret band.

The fluorescence spectra of **H_2P1** and **H_2P2** exhibit characteristic singlet state emission consisting of two vibronic bands, i.e. $Q(0,0)^*$ and $Q(0,1)^*$, in the range 550–800 nm (Fig. 12) [28]. In the fluorescence spectrum of **H_2TPP** two λ_{max} are observed at 652 and 716 nm, corresponding to $Q(0,0)^*$ and $Q(0,1)^*$ respectively, while the red shifted **H_2P2** exhibits bands at 658 and 723 nm and even more bathochromically shifted is the spectrum of **H_2P1** with bands at 666 and 722 nm. A fluorescence quantum yield (Φ_{fl}) of 0.006 was reported for **H_2P1**. This is less than the Φ_{fl} values of 0.010 and 0.120 reported for **H_2P2** and **ZnTPP** respectively. A similar trend was observed for the zinc metalled derivatives with **ZnP1** and **ZnP2** exhibiting emission bands occurring at 618, 658 and 605, 653 nm respectively. Fluorescence quantum yields of the metal complexes (**ZnP1**: 0.0013, **ZnP2**: 0.004) are also reduced when compared to **ZnTPP** (0.033). The decrease in quantum yield of **H_2P1** relative to **H_2P2** has been attributed to the closer proximity of the sulphur to the porphyrin π-system.

Table 2
Luminescence data of thien-2-yl porphyrins and **H_2TPP** in toluene at ambient temperature (τ_f = fitted fluorescence lifetime, Φ_{fl} = fluorescence quantum yield, k_f = rate of fluorescence) [30].

Porphyrin	τ_f (ns)	Φ_{fl}	k_f (1/ns)
H_2TPP	9.80	0.110	0.102
H_2P1	1.11	0.013	0.090
H_2P8	1.20	0.017	0.830
H_2P27	1.31	0.014	0.760
H_2P28	1.47	0.014	0.680

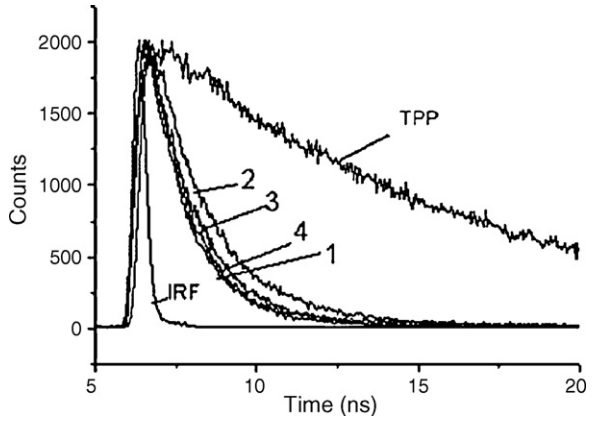

Fig. 13. Fluorescence decay signals of **H_2TPP**, **H_2P1** (1), **H_2P27** (3), **H_2P28** (2) and **H_2P8** (4) in toluene at ambient temperature. The detection wavelength is 660 nm. IRF indicates instrument response function [30].
Reproduced from reference [30] with permission of the copyright holders.

A reduction in singlet state lifetime was observed for the thienyl porphyrins **H_2P1** (Fig. 2), **H_2P8**, **H_2P27** and **H_2P28** (Fig. 10), with respect to **H_2TPP** (Table 2 and Fig. 13) [30]. This is attributed to the presence of the four "heavy" sulphur atoms on the periphery of the macrocycle; however suggestion of π–π overlap of the thiophene and porphyrin systems was also implied by the authors.

The fluorescence lifetimes of zinc(II)thienylporphyrins **ZnP8**–**ZnP13** (Fig. 4) are in the range 1.36–0.52 ns [21]. The shortest lifetime was that of **ZnP8**, having four heavy bromine atoms, and it also possessed the lowest quantum yield (Φ_{fl} = 0.006). The fluorescence emission spectra for **ZnP11**–**ZnP13** increase in intensity, with a concurrent red shift of their λ_{max} as the number of 5-trimethylsilylethynylthien-2-yl moieties increase, when compared to **ZnTPP**. The Φ_{fl} for the mono- and di-(5-trimethylsilylethynylthien-2-yl)porphyrins increase by 39% and 27% respectively. Triplet excited state $^3(\pi-\pi)$ absorption spectra and transient absorption lifetimes were also obtained. Similar to **ZnTPP**, each porphyrin displayed a weak absorption in the UV region with another more intense absorption in the visible region. In the case of **ZnTPP** a λ_{max} was observed at 470 nm, however with the *meso* tetrathien-2-ylporphyrins **ZnP11**, **ZnP12** and **ZnP13** the λ_{max} is observed in the region between 490 and 500 nm. A substantial increase in absorption, in the region 580–780 nm was also observed, which is attributed to charge transfer to the peripheral thein-2-yl π-system. A decrease in lifetime was observed for **ZnP1** (20 μs), **ZnP8** (7 μs), **ZnP9** (12 μs) and **ZnP10** (13 μs) relative to **ZnTPP** (24 μs). Increasing the number of 5-trimethylsilylethynylthien-2-yl moieties on the porphine macrocycle resulted in a decrease in lifetime. These excited state characteristics suggest a relatively strong coupling of the porphyrin ring and the thien-2-yl π-framework. Thus, the combination of studies by Brückner et al. and Rochford et al. have shown that considerable electronic communication between the porphyrin and thienyl π-systems exists in both the ground and excited states and that conclusions reached in earlier studies of these systems implying inductive effects alone needs to be revised.

In *trans* thienyl porphyrins, the classic electronic spectra of the porphyrin is retained although it is hypsochromically shifted compared to both **H_2P1** (Fig. 1) and **H_2TPP** [16]. The *trans* porphyrin, **H_2P7** (Fig. 3) displays an intense Soret band with a maximum absorbance at 411 nm, with Q bands displaying a similar blue shift. The emission spectrum of the *trans* porphyrin possesses a strong red fluorescence, centred at 642 nm with a weak shoulder at ~707 nm. The emission profile is very similar to that of **H_2TPP** (λ_{em} = 653, 721 nm) with only a slight blue shift.

The electronic absorption properties for porphyrins, **ZnP16**–**ZnP21** (Fig. 6), were examined (Table 3) and results indicate that both the λ_{max} of the Q bands and emission spectra depend on whether the thiophene moiety is linked to the porphyrin macrocycle directly at the *meso*-carbon position (**ZnP16**–**ZnP18**) or through an intervening ethynyl unit (**ZnP19**–**ZnP21**) and is also affected by the number of thiophene units (n = 1, 2 or 3, Fig. 6) [25]. Modest Stokes shifts (350–1300 cm^{-1}) imply that the derivatised porphrinatozinc(II) chromophores undergo modest to substantial excited state structural redistributions. This variance in Stokes shift is consistent with electronic structural effects within these molecules and also an appreciable quinoidal resonance contribution in the excited state. For each mode of connectivity, the chromophores that incorporate a single thiophene unit (**ZnP16** and **ZnP19**, n = 1) possess the largest Stokes shift within their class (1298 and 593 cm^{-1} respectively). The emission maxima of molecules in each class follow a similar trend, in that, they shift hypsochromically with increasing number of thiophene units. The porphyrins with thiophene units bonded directly at the *meso* position (**ZnP16**, **ZnP17** and **ZnP18**) display emission maxima values at 698, 669 and 662 nm respectively while the porphyrins linked to the thiophene through the ethynyl moiety show bathochromically shifted emission maxima which shift hypsochromically with increasing thiophene units at 714, 706 and 700 nm for **ZnP19**, **ZnP20** and **ZnP21** respectively. This is indicative of the increased excited-state electronic dipole moment due to extensive porphyrin–thiophene conjugation. Hyper-Rayleigh scattering (fs-HRS) was used to determine the hyperpolarisability

Table 3
Electronic data of **ZnP16**–**ZnP25** recorded in THF [25].

Porphyrin	Number of thiophene units	λ_{max} Soret (nm)	Q bands (nm)	Stokes shift (cm^{-1})	λ_{em} (nm)	β_{1300} (10^{-30} esu)
ZnP16	**1**	456	580, 640	1298	698	2400
ZnP17	**2**	457	583, 641	653	669	2200
ZnP18	**3**	458	579, 641	495	662	4335
ZnP19	**1**	465	685	593	714	690
ZnP20	**2**	468	683	477	706	670
ZnP21	**3**	470	683	356	700	1170
ZnP22	**1**	461	676	425	696	1020
ZnP23	**1**	469	698	1151	759	785
ZnP24	**1**	458	674	812	713	810
ZnP25	**1**	459	665	375	682	1400

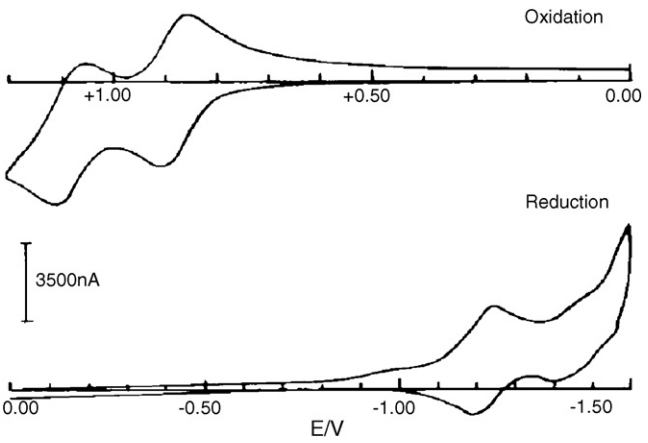

Fig. 14. Cyclic voltagram of **ZnP1** in CH_2Cl_2 *vs.* Ag/AgCl with 0.1 M TBAHFP as supporting electrolyte [8].
Reproduced from reference [8] with permission of the copyright holders.

values for porphyrins **ZnP18**, and **ZnP22**–**ZnP25** (Fig. 6) (this will be discussed later in Section 6).

Okada et al investigated substituent control of J-aggregate formation in water-insoluble porphyrins [33]. Working primarily with phenyl substituted porphyrins it was found that substituents at the *meso* position affected aggregation to a higher extent. Porphine and octaethylporphyrins did not form J-aggregates, indicating that aromatic rings at the *meso* position are necessary for aggregate formation. Furthermore, aromatic rings with large steric bulk also did not aggregate. In protonated solution, however **H_2P2** (Fig. 2) did form J-aggregates. This is evidenced by changes in the absorption spectra. The Soret band of the free base monomer (420 nm) is first replaced by the protonated monomer absorption (447 nm) which is in turn exchanged by a new absorption at 481 nm. Simultaneously the observed Q band at 652 nm is red shifted to 678 nm and subsequently to 756 nm. These bathochromic shifts in the absorption signify the assembly of "head-to-tail" aggregates. In most cases, AFM images of the J-aggregate films revealed square rod-like microcrystals. The Q band absorption of the aggregates varies widely from 658 to 756 nm while the Soret band remained around 480 nm. It was also noted that the electron-donating character of the *meso* substituents affected the FWHM of the Q bands: increasing the electron donating character caused increased FWHM measurements. These changes in the absorption spectra suggest that the energy levels of the excited states of the porphyrin J-aggregates are substituent dependant.

2.3. Electrochemical properties and electropolymerisation

It is possible by monitoring shifts in the anodic and cathodic redox processes, to determine the influence of the thienyl group on the HOMO and LUMO energies of the porphyrin. Each of the thienyl porphyrins, **H_2P1**, **H_2P2** and their zinc and copper analogues (Fig. 2), show two successive one-electron oxidations and two successive one-electron reductions (Fig. 14) [8]. **H_2TPP** was also examined to delineate the effect of the thienyl groups. The observed redox potentials revealed striking differences for **H_2P1** relative to **H_2P2** and **H_2TPP**. Both thienyl porphyrins show a cathodic shift of the first oxidation (50 mV for **$H_2P1^{+/0}$** and 110 mV for **$H_2P2^{+/0}$**). The first reduction of **H_2P2** is within experimental error comparable to **H_2TPP**; however **$H_2P1^{0/-}$** shows a substantial anodic shift of 140 mV which is primarily responsible for its reduced band gap and lower energy absorption. A HOMO–LUMO energy gap of 1.98 eV is calculated for **H_2P1** compared to 2.18 eV for to **H_2P2** and 2.23 eV for **H_2TPP**. Similar trends were observed for the metallated analogues with the **ZnP2** and **CuP2** redox potentials approaching those of **ZnTPP** and **CuTPP**. Although attributed to inductive effects by the authors this band gap narrowing observed upon thienyl substitution corresponds well with the ground and excited state photophysical trends discussed above by Brückner et al. and Rochford et al. and similarly can be explained by π–π overlap of the porphyrin and thienyl structures resulting in stabilisation of both HOMO and LUMO orbitals. In contrast to the previous results, **H_2P1** (Fig. 2), **H_2P8**, **H_2P27** and **H_2P28** (Fig. 10) showed two one-electron oxidations and only one, one-electron reduction process [30].

Substitution of the thien-2-yl moiety causes significant changes in the redox potentials as observed in the cyclic voltammetry studies on **ZnP8**–**ZnP13** (Fig. 4) [21]. All *meso* tetra(thien-2-yl)porphyrins show an anodic shift in their first oxidation (**$ZnP1^{+/0}$** 0.43, **$ZnP8^{+/0}$** 0.61, **$ZnP9^{+/0}$** 0.49, **$ZnP10^{+/0}$** 0.49 V *vs.* Fc/Fc^+) when compared to **$ZnTPP^{+/0}$** (0.34 V *vs.* Fc/Fc^+) indicating a stabilisation of the HOMO orbital of the porphyrin ring system. Stabilisation of the LUMO orbitals also occurs with a decrease in the potential of the first reduction. Again **ZnP8** showed the largest effect with a decrease in its reduction potential of 240 mV compared to **ZnTPP**. Increasing stabilisation of the HOMO and LUMO is observed on increasing the number of thienyl substituents on the porphyrin ring in **ZnP11**, **ZnP12**, **ZnP13** and **ZnP9**, which appears to be the dominant factor in reducing the calculated HOMO–LUMO energy gap for these systems. This reduction in band gap follows the order **ZnP9** (2.02 eV) < **ZnP13** (2.02 eV) < **ZnP12** (2.04 eV) < **ZnP11** (2.06 eV) < **ZnTPP** (2.09 eV). Thus by controlling the number of thienyl substituents on the porphyrin, as well as the nature of substituent on the thienyl ring itself, the band gap can be manipulated.

It is well established that the HOMO orbital of the porphyrin macrocycle is destabilised upon reduction of its planarity, which thus lowers the HOMO–LUMO energy gap [34]. This is realised in the redox properties of the copper(II) metallated derivatives of the highly substituted porphyrins, **CuP3**, **CuP4** and **CuP5**, along with **CuP1** (Fig. 2) [10]. Substitution of the porphyrin ring with thien-2-yl moieties in the *meso*- and β-positions increased the energy of the HOMO orbital as expected, however a stabilisation of the LUMO orbital also occurred resulting in an overall decreased energy gap of 1.89 eV for **CuP4**, 1.63 eV for **CuP3** and 1.48 eV for **CuP5**. HOMO–LUMO energy gaps of 2.34 eV and 2.20 eV were reported for **CuTPP** and **CuP1**.

Two reversible waves occur at −1.58 V and −2.04 V *vs.* SCE for *trans* dithienylporphyrin (**H_2P7**, Fig. 3) [16]. Continual sweeps of the dithienylporphyrin resulted in the deposition of a thin insoluble polymer on the electrode. Further investigation of this polymer layer confirmed that it belongs to the restricted family of "zero bandgap" polymers, that is, the onset oxidation potential is less than or equal to the onset reduction potential. Porphyrins with band gaps as low as 0.80 and 0.35 eV have previously been reported [35]. This *trans* dithienyl porphyrin is the first "zero bandgap polymer" in a poly(aryl-porphyrin) series. The authors are continuing physiochemical studies in order to explain such electrochemical behaviour.

The iron (III) porphyrin **Fe(III)P2** (Fig. 2) also undergoes electropolymerisation [23]. An anodic wave at ~1.30 V *vs.* Ag/AgCl was attributed to oxidation of the peripheral thien-3-yl groups in the monomer and a subsequent single broad anodic wave in the region 1.0–1.5 V *vs.* Ag/AgCl signifies polymerisation of a porphyrin film (**poly-FeP2**, Fig. 15) onto the electrode. The electrode modified with **poly-FeP2** demonstrated electroactivity due to the presence of the iron(II/III) couple and a mean redox potential of 0.0 V *vs.* Ag/AgCl suggests a low charge transfer resistance within the semiconductive film. The bromoiron(III) *meso* tetrakis(thien-3-yl)porphyrin was coordinated with the axial ligand, 1-methylimidzole (im), to form the coordination complex **$[Fe(im)P2]^+Br^-$**. Electrodeposition

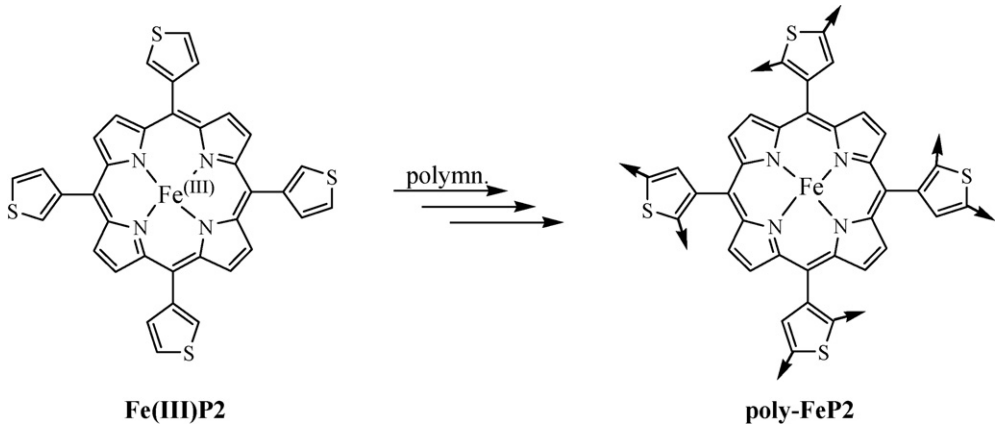

Fig. 15. Polymerisation of **Fe(III)P2** [23].

of the complex resulted in a broad anodic wave in the range 0.8–0.15 V *vs.* Ag/AgCl and the polymerised complex was electroactive with a mean redox potential of −0.05 V *vs.* Ag/AgCl.

The metalloporphyrins (M = Zn, Pd) **MP14** and **MP15** (Fig. 5) were polymerised by electrochemical oxidative coupling of the *meso* oligothienyl groups [24]. The repeated oxidation of *meso* bithienyl groups of **ZnP14** was observed above 1.40 V *vs.* SCE, with the redox couple of the first oxidation of the porphyrin ring (observed at *ca.* 1.0 V) increasing with increasing number of cycles. During the experiment the polymer (**poly-ZnP14**) deposited onto the working electrode. Electrochemical polymerisation of **ZnP15** (oxidation of the porphyrin ring: 0.60 V *vs.* SCE, oxidative coupling of terthienyl groups: 0.71–0.80 V *vs.* SCE) and the palladium complexes of bithienyl and terthienyl substituted porphyrin was achieved in a similar manner. Infra-red analysis indicated that α–α coupling of the *meso*-oligothienyl groups occur to form a quasi-2D polymer (Fig. 16). Scanning tunnelling microscopy (STM) of an ultra thin film of **poly-ZnP15** prepared on an Au(III) substrate confirmed a quasi-2D structure, although some disorder was included. Film thickness of 0.5 nm indicates a planar orientation of the porphyrin rings, with an alternating structure of porphyrin and oligothiophene moieties. The mean distance between the intersections was *ca.* 2.82 nm and the model distance between the monomer units was *ca.* 3 nm, thus supporting that **poly-ZnP15** forms a lattice. The d.c. conductivities of **poly-ZnP14** and **poly-PdP14** were 3×10^{-7} S/cm and 2×10^{-7} S/cm respectively. Layered polymers cells (ITO electrode/**poly-PdP14**/**poly-ZnP14**/Au electrode), constructed by the successive electrochemical polymerisation of **PdP14** and **ZnP14** showed electric rectifying properties. As the contacts between the individual polymers and the electrodes

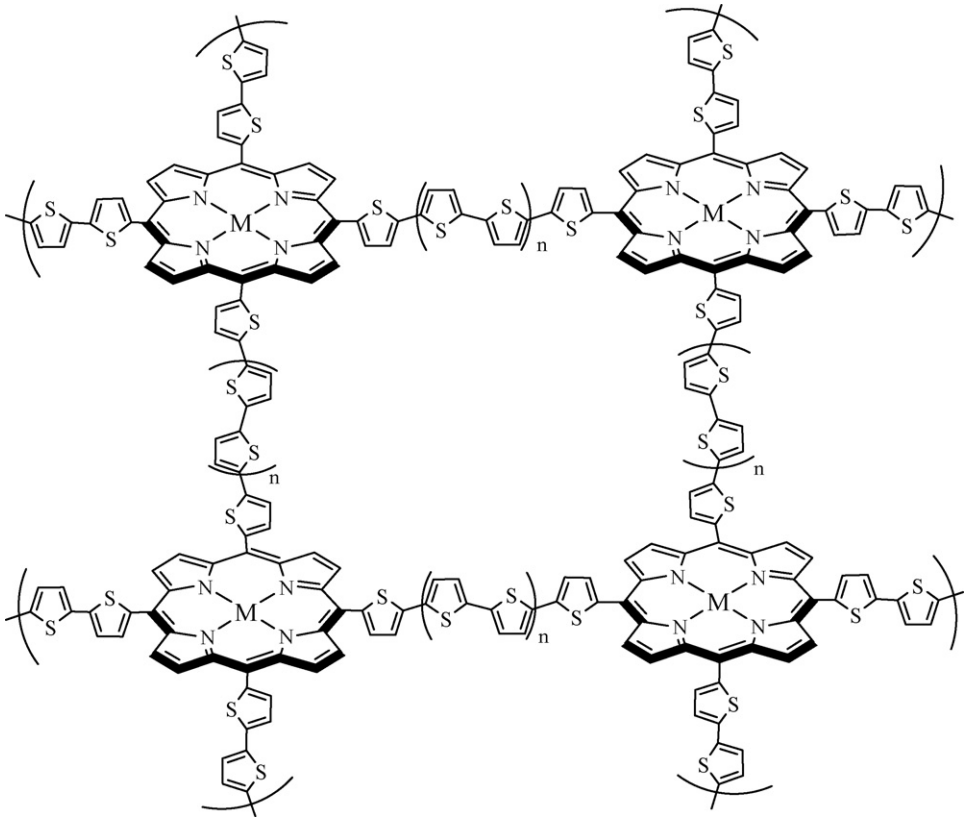

Fig. 16. Proposed quasi 2D structures of **MP14** and **MP15** where M = Zn(II) or Pd(II) and $n = 2$ [24].

are ohmic, the rectifying properties are thought to arise from the molecular interface between **poly-ZnP14** and **poly-PdP14** [36].

3. Indirectly appended thienyl porphyrins (thiophene attachment *via* saturated/unsaturated groups or axial coordination)

3.1. Synthesis

Crossley and Prashar reported the design and synthesis of a series of thiophene appended porphyrins (**H_2P29**–**H_2P33**, Fig. 17) where the thiophene ring is fused to the periphery of the macrocycle *via* two aza linkages [37]. The aim of their work was to attach highly conjugated porphyrins to a gold surface through the sulphur atom of the fused thiophene ring in order to study the self assembly and molecular electronic properties of porphyrin based monolayers and thin films.

Naphtoporphyrin systems using a series of pyrroles fused with aromatic rings (isoindole derivatives) were reported by Ono et al. [38]. The aromatic nitro compound **1** (Scheme 2), was reacted with ethylisocyanoacetate in the presence of DBU to give fused pyrrole **2**, in 60% yield. Reduction of **2** to the hydroxymethyl pyrrole, **3**, is a crucial step in the reaction. Tetramerisation and oxidation of compound **3** led to the production of **H_2P34**. Suppression of scrambling proved difficult with a mixture of four regioisomers produced, the main product of which was the type I porphyrin **H_2P34** (Scheme 2). Only suitably controlled conditions for reduction and tetramerisation allowed the isolation of **H_2P34**. A similar fused porphyrin–thiophene system (**ZnP35**, Fig. 18) was reported by Callot and co-workers [39].

3′-[5-(4-Phenoxy)-10,15,20-tritolylporphyrin]-2,2;-bithiophene (**H_2P36**, Fig. 19) and 3′-[5-(4-Phenoxy)-10,15,20-tritolylporphyrin]pentyl-2,2′:5′,2″-terthiophene (**H_2P37**, Fig. 19) were synthesised by coupling the porphyrin subunit [5-(4-phenoxy)-10,15,20-tritolylporphyrin)] to the relative oligothiophene by a Williamson ether synthesis to yield the tetraphenylporphyrin

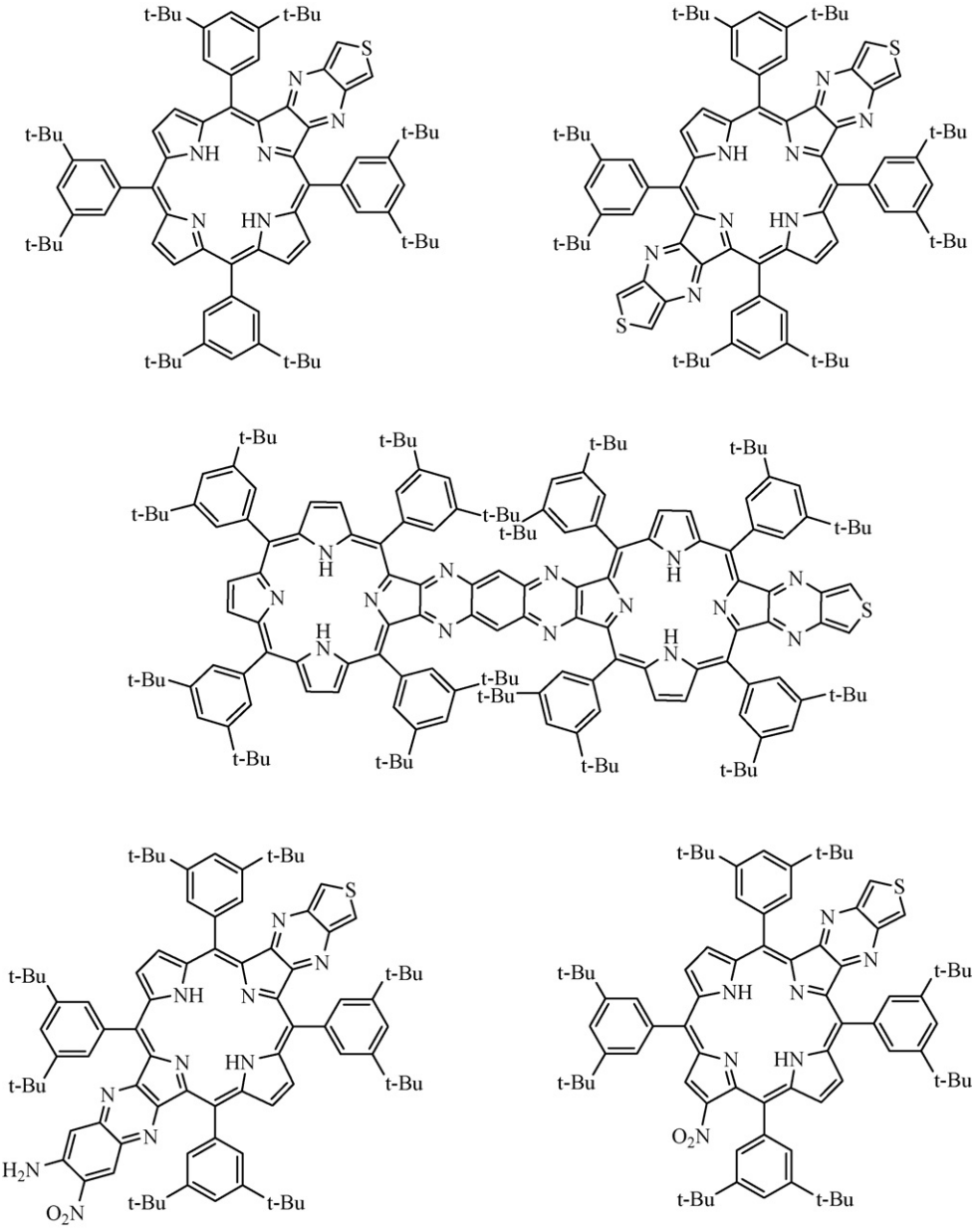

Fig. 17. Crossley and Prasher's fused thienyl porphyrins **H_2P29**–**H_2P33** [37].

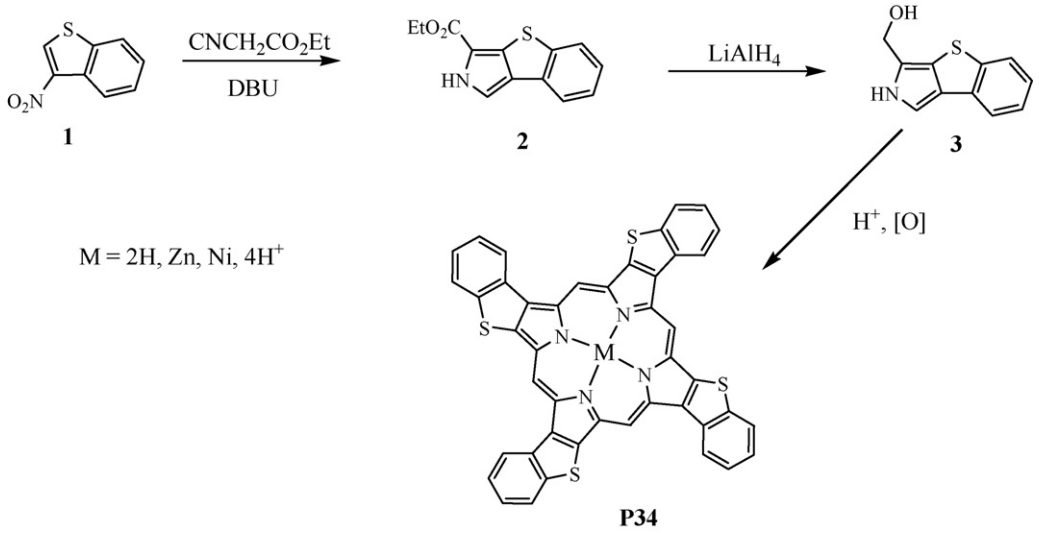

Scheme 2. Synthesis of **P34** [38].

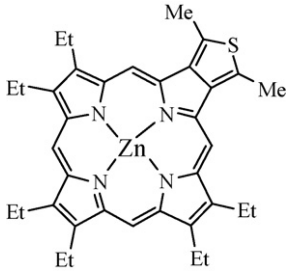

Fig. 18. ZnP35 [39].

functionalised bithiophene and the analogous terthiophene [40]. The corresponding cobalt, nickel, zinc, iron and manganese complexes were also isolated (Fig. 19). In another study 5-(4-(1-hexylthien-3-yl)phenoxy)-10,15,20-tritolylporphyrin (**H_2P38**, Fig. 19) and the corresponding porphyrin without the thienyl group (5-(4-(1-Hexyl)phenoxy)-10,15,20-tritolylporphyrin were synthesised by the Adler–Longo method. The thienyl porphyrin **H_2P38** was also metallated with nickel in high yield [41].

On reacting a thiophene substituted benzaldehyde with 5-phenyldipyrromethane, the free base 5,15-bis(4-(2-(3,4-ethylenedioxy)thienyl)phenyl)-10,20-diphenylporphyrin (**H_2P39**, Fig. 20) and 5,15-bis(4-(2-thienyl)phenyl)-10,20-diphenylporphyrin

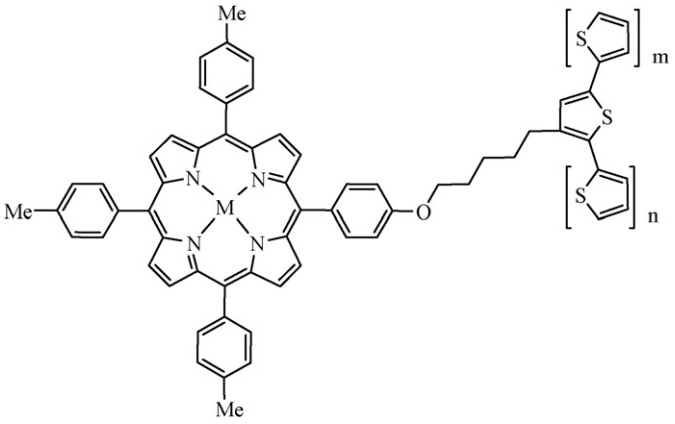

Fig. 19. P36: $m = 1$, $n = 0$, M = Zn(II), Ni(II), Co(II), Fe(III)Cl, Mn(III)Cl. **P37**: $m = 1$, $n = 1$, M = Ni(II), Co(II), Fe(III)Cl. **P38**: $m = 0$, $n = 0$, M = 2H, Ni(II) [40,41].

(**H_2P40**, Fig. 20) and their metal analogues were isolated [42]. The thiophene and 3,4-ethylenedioxythiophene moieties were chosen as polymerisation points on the porphyrin monomers as shown in Fig. 27.

A number of phosphoric, P(V) porphyrin derivatives with two thienylalkoxy or oligothienylalkoxy groups at the axial position of the central metal atom were also synthesised [43]. The donor–photosensitiser–acceptor molecules were synthesised from dichlorophosphoric(V)-tetraphenylporphyrin and the corresponding thienyl or oligothienyl alcohol. Spectroscopic analysis confirmed that the two equivalent alkoxy groups were attached to the central phosphorus atom at the fifth and sixth coordination position (Fig. 21).

Zinc(II)-porphyrin polymers with *meso*-linked aryl and ethynyl spacers were synthesised using a combination of Stille and Sonogashira palladium coupling and $Ni(cod)_2(bpy)$ [cod = 1,5-cyclooctadiene] [22]. The porphyrin monomers **H_2P44**–**H_2P48** were synthesised by the MacDonald 2 + 2 reaction of bispyrrole and a range of aldehydes, followed by metallation with zinc yielding **ZnP44**–**ZnP48** (Fig. 22). The porphyrin monomers were directly coupled to form homopolymers and also coupled to aryl units to form copolymers.

The oligothienyl linkage in multicomponent porphyrin systems is of great importance with two roles; firstly it functions as a rigid spacer, positioning two neighbouring centres at a fixed distance with a well defined geometry. Secondly the spacer can promote electronic communication, thus facilitating electron and/or energy transfer between two porphyrins. For this reason Odobel and co-workers synthesised a series of oligothiophene bridged bisporphyrins (Fig. 23), with the oligothiophene tethered by a single, double (*trans*) or triple bond to the *meso* position [44]. The porphyrins were produced by palladium catalysed cross coupling reactions (Stille, Heck and Sonogashira) between 5-iodo-10,15,20-(3,5-di*tert*-butylphenyl)porphyrin and the oligothienyl chain.

The synthesis of freebase and Zn(II) 5,15-bis(acetylene-4-(ethylenedioxy)thiophene)-10,20-bis(4-methoxycarbonylphenyl)porphyrins (**H_2P53** and **ZnP53**, Fig. 24) and their hydrophilic disodium dicarboxylate derivatives (**H_2P54** and **ZnP54**, Fig. 24) have also been reported [45]. The porphyrin monomer synthesis begins with Sonogashira coupling of 2-iodo-3,4-(ethylenedioxy)thiophene with 3,3-diehtoxypropyne, followed by cyclisation with 5-(4-methoxycarbonylphenyl)dipyrromethane to give the porphyrin, **H_2P53**.

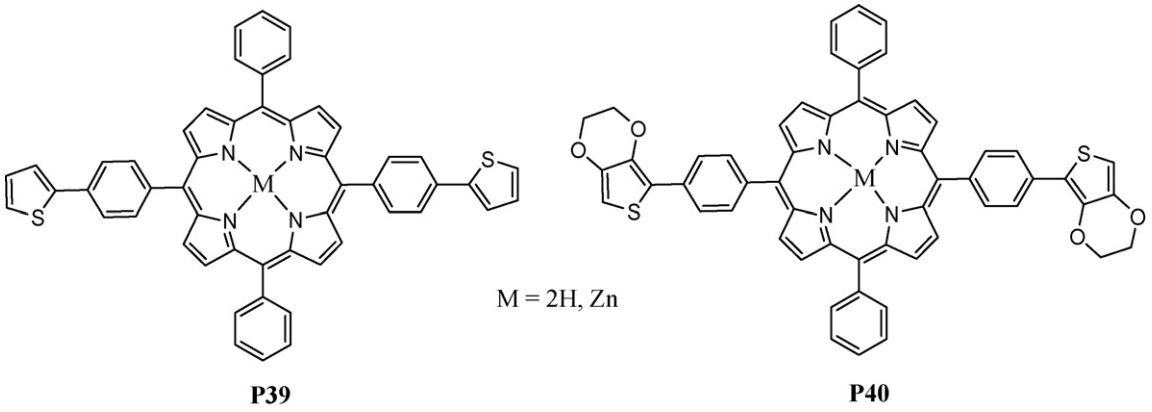

Fig. 20. Porphyrin monomers **P39** and **P40** [42].

Kuo et al. presented a novel synthetic route to zinc tetrakis(arylethynyl)porphyrins [46]. Using adapted Sonogashira methods, a range of electron donating substituents were coupled with 5,10,15,20-tetrakis(ethynyl)porphyrin and their redox properties examined. In this manner, they produced zinc(II) 5,10,15,20-tetrakis(thien-2-ylethynyl)porphyrin, **ZnP55** (Scheme 3).

The crystal structure of a porphyrin dimer linked by an unsaturated bridge containing a thiophene unit was also obtained (Fig. 25) [47]. The thiophene bridged dimer, **NiP56**, showed distortion of the bond angles in the diethynylthiophene unit, with the porphyrin moieties bending away from the sulphur side of the ring. The result is that the two triple bonds are almost co-linear. This clearly demonstrates strong π-overlap across the bridge. Ruffling of the porphyrin core is also observed with Ni–N distances of 1.91 Å, which are typical of those reported for distorted nickel porphyrin structures.

3.2. Electronic and photophysical properties

The extended π-system in the porphyrins with fused aromatic rings, **H_2P34** (Scheme 2), leads to a red shift for both the Soret and Q bands [38]. The Soret band in **H_2P34** was observed at 432 nm compared to 417 nm for **H_2TPP**. In order to compare the extent of π-conjugation between the porphyrin ring and the fused aromatics the absorption spectrum of the diprotonated species was obtained. The Soret and Q bands are again both red shifted, the former more so than the latter. The diprotonated species displays a Soret band at 462 nm with Q bands at 604 and 659 nm. Soret bands for the analogous **ZnP34** and **NiP34** porphyrins were also bathochromically shifted to 438 nm and 452 nm respectively.

Decoupling of the two chromophores by the oxaalkyl spacer was observed in the electronic spectrum of **H_2P36** and **H_2P37** (Fig. 19) [40]. The spectral features consist of an intense Soret band at 420 nm with Q bands between 510 and 650 nm due to the porphyrin and a π–π^* transition between 290 and 350 nm due to the oligothiophene. The Soret band in **ZnP36** is bathochromically shifted by 2 nm compared to its freebase analogue (λ_{max} = 420 nm), whereas the **CoP36**/**37** and **NiP36**/**37** display hypsochromically shifted Soret bands at 412 and 416 nm respectively. The trivalent metal complexes show highly red shifted Soret bands (**Fe**(**III**)**P36**: 511 nm, **Fe**(**III**)**P37**: 512 nm, **Mn**(**III**)**P36**: 480 nm) with respect to the freebase porphyrins **H_2P36**/**H_2P37** (λ_{max} = 420 nm) with an additional intense absorption between 350 and 400 nm, assigned to charge transfer of occupied π-orbitals of the porphyrin to vacant d-orbitals of the central metal cation.

The metallated phosphoric(V) porphyrins with axial substituents also display the classic porphyrin spectrum with additional spectral features due to the axial thienyl moiety at 232, 310 and 357 nm for **P**(**V**)**P41**, **P**(**V**)**P42** and **P**(**V**)**P43** (Fig. 21) respectively [43]. Soret bands were observed at 430 nm, 428 nm and 431 nm respectively for **P**(**V**)**P41**, **P**(**V**)**P42** and **P**(**V**)**P43** with the two Q bands of each porphyrin in the range 558–604 nm.

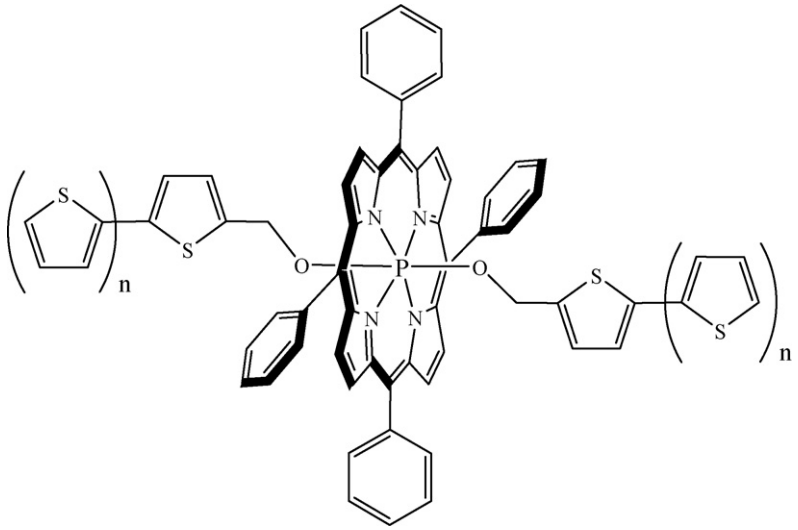

Fig. 21. **P**(**V**)**P41**: n = 0, **P**(**V**)**P42**: n = 1, **P**(**V**)**P43**: n = 2 [43].

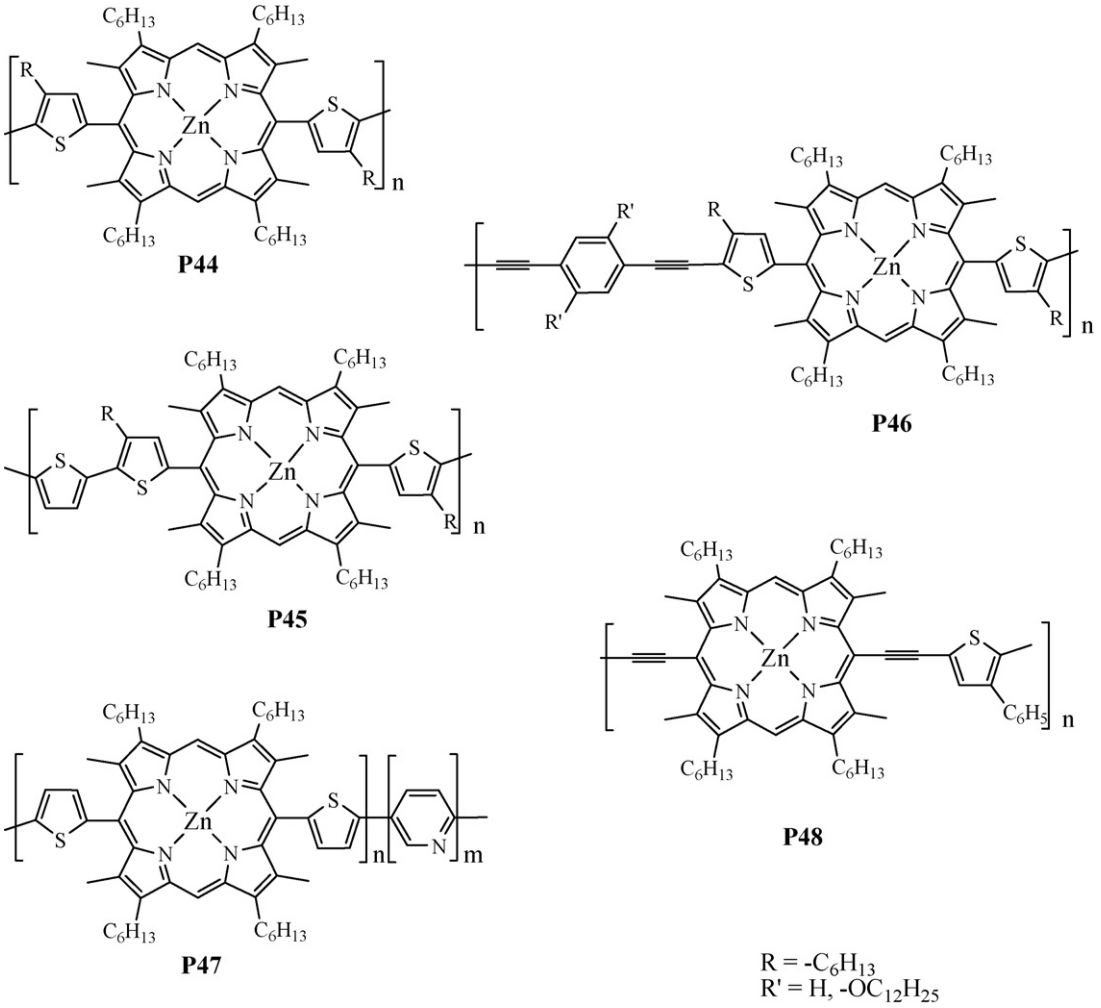

Fig. 22. Thienyl porphyrins with *meso*-linked aryl and ethynyl spacers [22].

The fluorescence quantum yields and lifetimes in these systems are dependent on the number of thiophene units in the system (Table 4), with a decrease in the fluorescence lifetime and quantum yield with increasing number of thiophene units. Surprisingly the **P**(**V**)**P42** system showed a larger decrease in fluorescence lifetime and quantum yield than the **P**(**V**)**P43** analogue. Fluorescence quenching was observed for **P**(**V**)**P42** and **P**(**V**)**P43**, compared to diethoxyP(V)tetraphenylporphyrin (τ = 4.4 ns) without thienyl moieties attached, which indicates that photoinduced electron transfer occurs from the oligothiophene moiety to the P(V)porphyrin unit of the 2,2′-bisthiophene and 2′,2″:5″,2‴-terthiophene systems.

In the ethynyl-thienyl porphyrin, **ZnP55** (Scheme 3), both the absorption and emission maxima are bathochromically shifted

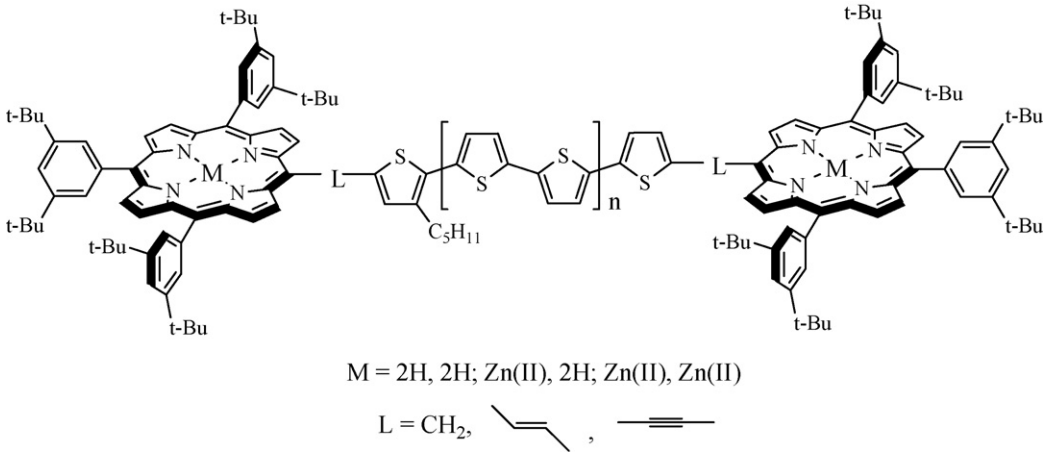

Fig. 23. P49: n = 0, L = CH_2. **P50**: n = 1, L = CH_2. **P51**: n = 1, L = *trans* vinyl link. **P52**: n = 1, L = ethynyl link [44].

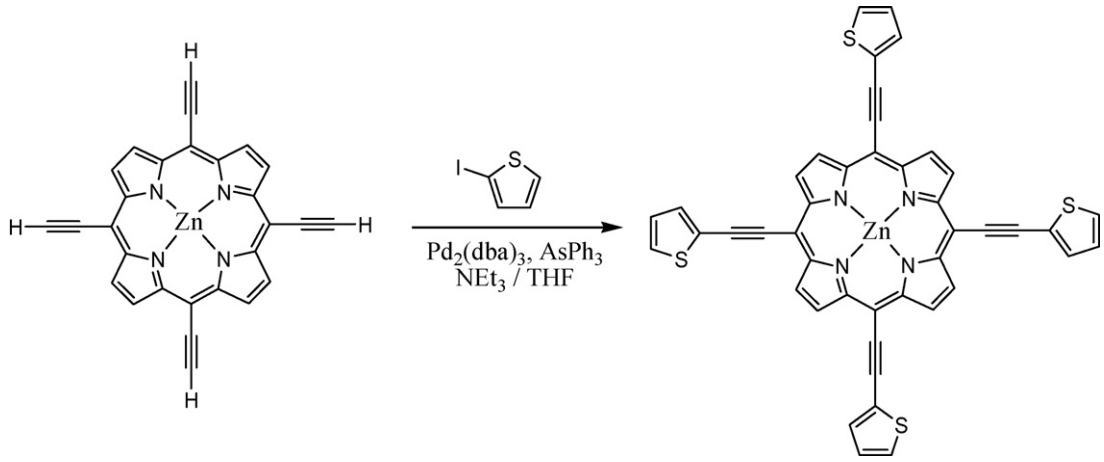

Scheme 3. Novel route to **ZnP55** [46].

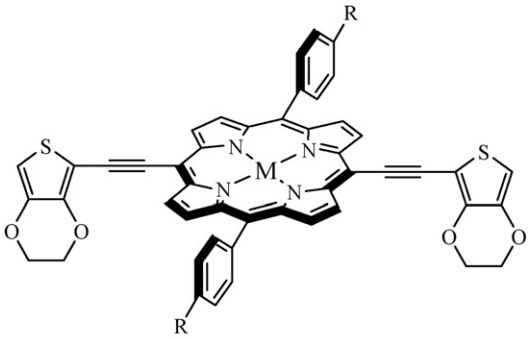

Fig. 24. P53: R = $COOCH_3$. **P54**: R = COO^-Na^+ [45].

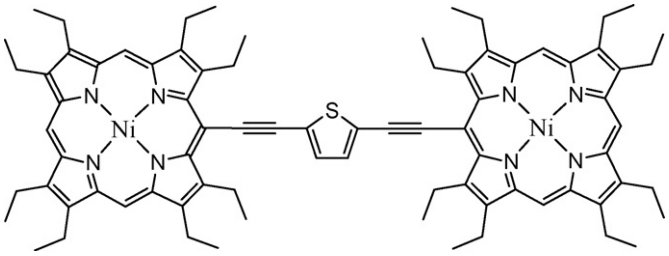

Fig. 25. Structure of **NiP56** [47].

compared to **H_2P1** (Fig. 2) [46]. The Soret band maximum was detected at 484 nm with a Q band at 691 nm, and the emission bands were observed at 703 and 774 nm.

The electronic spectra of the porphyrin systems connected with four types of oligothiophene bridges (Fig. 23) show many interesting characteristics [44]. **ZnZnP49** and **ZnZnP50** display the least perturbation when compared to the reference porphyrin, zinc(II)5,15-bis(3,5-di*tert*-butylphenyl)porphyrin, as their spectra are simply the sum of the porphyrin and the oligothiophene bridge. Inserting the vinyl or ethynyl linker between the quaterthiophene moiety and porphyrin core as in **ZnZnP51** and **ZnZnP52** imparts distinctive features to the absorption spectra. The Soret bands are broadened compared to both **ZnZnP49** and **ZnZnP50** while the Q bands are red shifted with a considerable increase in intensity. **ZnZnP52** undergoes the largest red shift and highest intensification of Q bands within the series, which is attributed to the effect of the ethynyl substituent. The changes evident in the spectra are a result of a decrease in the HOMO–LUMO gap as a consequence of increased π-conjugated in the system. The Soret region of **ZnZnP52** is split into two discernible transitions, at 437 and 448 nm with a shoulder at 417 nm indicative of J-aggregate formation. **H_2H_2P52** and **ZnH_2P52** display single maxima at 442 and 444 nm respectively. Also a 20% increase in the FWHM of the Soret band in **ZnZnP52** is observed compared to the other porphyrins in the **P52** series. The Q band region of **ZnH_2P52** is the sum of the spectra for **ZnZnP52** and **H_2H_2P52**. However the smaller vinyl moiety in the bridge of **ZnZnP51**, **H_2H_2P51** and **ZnH_2P51** results in red shifted Q bands, thus indicating that interaction occurs through the smaller vinyl group. Both vinyl and ethynyl substitution at the *meso*-position gave rise to enhanced coupling between the two porphyrin units in comparison to the directly linked quaterthiophene bridge which only displayed weak interactions indicating only slight perturbation of the ground state properties of the porphyrin units. Similar to the absorption spectra, the fluorescence spectra are altered by the nature of the bond linking the porphyrin units to the bis- or quaterthiophene bridge (Table 5). The fluorescence quantum yields for the zinc dyads increase in the order **ZnZnP50** < **ZnZnP49** < **ZnZnP51** ≈ **ZnZnP52**. The fluorescence quantum yields for the **H_2H_2** porphyrin series

Table 4
Luminescence data for phosphoric(V) porphyrins **P41**–**P43** in MeCN [43].

Porphyrin	λ_{em} (nm)	τ_f (ns)	Φ_{fl}
P(V)P41	613, 668	4.10	2.7×10^{-2}
P(V)P42	615, 668	<0.5	5.1×10^{-4}
P(V)P43	622, 673	0.80	3.9×10^{-3}

Table 5
Luminescence data for porphyrin dimers **P49**–**P52** in THF [44].

Porphyrin	λ_{em} (nm)	τ_f (ns)	Φ_{fl}
ZnZnP49	624	1.60	0.10
ZnH_2P49	664	0.02	0.86
H_2H_2P49	662	3.90	0.86
ZnZnP50	626	1.30	0.09
ZnH_2P50	666	0.03	0.78
H_2H_2P50	667	3.50	0.78
ZnZnP51	676	1.30	0.17
ZnH_2P51	713	0.03	0.21
H_2H_2P51	717	3.40	0.22
ZnZnP52	657	1.40	0.18
ZnH_2P52	688	0.01	0.31
H_2H_2P52	690	6.20	0.34

Table 6
Electronic data for **P44**–**P48** in $CHCl_3$ [22].

Porphyrin	λ_{max} Soret (nm)	λ_{max} Q bands (nm)	λ_{ex} (nm)	λ_{em} (nm)
ZnP44	417	542, 583	417	592, 644
Poly-ZnP44	416	543, 582	416	590, 642
Poly-ZnP46	416	546, 584	416	590, 639
Poly-ZnP47	417, 431	547, 585	422	591, 646
Poly-ZnP48	454, 490	697	455	724

follow a similar trend. The largest Stokes shift between the lowest absorption band and the fluorescence maxima is observed for **H_2H_2P51**, **ZnZnP51** and **ZnH_2P51**, indicating that the **P51** series undergo a significant reorganisation of nuclear coordinates in the excited state. The energy transfer in the asymmetrical systems was also studied by fluorescence spectroscopy. Photoinduced energy transfer between asymmetrical **ZnH_2** porphyrins dyads was investigated. The lowest singlet excited state (S_1) of the zinc porphyrin is higher than that of the corresponding freebase porphyrin. Excitation of the asymmetrical dyad at 560 nm (the wavelength at which most of the light is absorbed by the zinc unit) produces a fluorescence spectra with >95% of emission from the freebase porphyrin. This indicates efficient energy transfer from the zinc porphyrin excited state to the nearby freebase porphyrin. The decrease in the zinc porphyrin fluorescence lifetime indicates a clear trend in energy transfer from the slowest to the fastest of the order **ZnH_2P50** ≈ **ZnH_2P51** > **ZnH_2P49** > **ZnH_2P52**. Although the interporphyrin distance is greatest in **ZnH_2P52**, it has the fastest energy transfer rate indicating the good electronic communication, mediated by the bridge.

Electronic coupling between the adjacent porphyrin units in the polymer backbone of **poly-ZnP47** and **poly-ZnP48** (Fig. 22) resulted in splitting of the Soret band in the UV–vis spectra (Table 6) [22]. The monomer **ZnP44** displays a sharp Soret peak at 417 nm with FWHM of *ca.* 1151 cm^{-1}. Polymers **poly-ZnP44**, **poly-ZnP46**, **poly-ZnP47** and **poly-ZnP48** gave peaks in the Soret and Q bands region, the sharpness and intensity of which depended on the structure of the polymer. **Poly-ZnP48** with an ethynyl spacer directly bound to the *meso* position of the porphyrin ring displayed the largest shift for all Soret bands in the series. Polymers which have a spacing thiophene unit directly bonded to the zinc porphyrin units, such as **poly-ZnP44**, **poly-ZnP46** and **poly-ZnP47** (Fig. 22) display two emission bands which are similar to those of the relative monomers. In accord with its UV–vis spectrum, the photoluminescence of **poly-ZnP48** is at a longer wavelength than the other polymers.

A Soret band with a λ_{max} at 460 nm was observed for **ZnP53** (Fig. 24) in dichloromethane, while **poly-ZnP54** displayed a hypsochromically shifted Soret band at 434 nm in dimethylsulfoxide [45]. Two fluorescence bands were observed for **poly-ZnP53** and **poly-ZnP54** at 650, 720 nm and 620, 660 nm respectively, whereas an intense single fluorescence band was observed at 720 nm for **ZnP53**.

3.3. Electrochemical properties and electropolymerisation

HOMO–LUMO energy gaps of 2.06 and 2.01 eV were calculated for **ZnP34** and **NiP34** (Scheme 2) respectively [38]. These values correspond to a reduced HOMO–LUMO energy gap of almost 30 eV relative to **ZnTPP**. Cyclic voltammetry studies carried out on **H_2P36** and **H_2P37** (Fig. 19) reveal potentials comparable to the individual subunits which are in agreement with the UV–vis studies, confirming a lack of electronic communication [40]. Polymerisation of the freebase porphyrin monomer units, **H_2P36** and **H_2P37**, was not possible due to the interference of the porphyrins internal nitrogens with the oligothiophene radical cations. However electrochemical oxidation of the metallo-porphyrins lead to the corresponding porphyrin functionalised polythiophene. The bisthiophene analogues coordinated with divalent and trivalent metals, M(II)/M(III)**P36**, showed a higher tendency to polymerise and also gave thicker films. Only **Mn(III)P36** displayed low polymerisation trends. Electrochemical studies on the polymers displayed a combination of reversible redox waves for the conducting polythiophene backbone and the porphyrin redox centres (Table 7). Reduction of the metal centres of the porphyrin units at negative potentials was not observed due to the insulating character of the polythiophene backbone in the potential window monitored.

In contrast, Ballarin et al. observed irreversible oxidation of the porphyrin moiety in a copolymer of **H_2P36** and the tetraphenylporphyrin-alkoxy-monothiophene unit, **H_2P37** [41a]. In a later study [41b], the authors also investigated the Ni derivative, **NiP36**, and analysed the complexation ability of the porphyrin unit in the polymer chain. Both **H_2P36** and **NiP36** form mechanically stable electrode surface films. For **H_2P36** the oxidation process centred at +1.04 V *vs.* SCE, previously ascribed to the oxidation of the porphyrin-containing monomer, was observed along with an additional redox couple in the region +0.45 to +0.70 V attributed to oxidation of the co-polymer. Analysis of **NiP36** was quite different. The oxidation process recorded for **H_2P36** was no longer present and a reversible system was evident with an oxidation potential of +0.94 V *vs.* SCE. This shift with respect to **H_2P36** was attributed to the nickel porphyrin core, however the highly distorted conformation of the porphyrin ring induced upon nickel(II) complexation should also be considered.

One dimensional polymers were formed *via* electrochemical oxidation of **P(V)P42** and **P(V)43** (Fig. 21) [43]. **Poly-P(V)P42** and **poly-P(V)43** were deposited onto the electrode as peak currents assigned to the redox reaction of the P(V) porphyrin increased. **Poly-P(V)P43** displayed a new anodic peak due to the oxidation of sexithiophene. The UV–vis absorption of the bithiophene

Table 7
Redox potentials of the **P36** and **P37** series in CH_2Cl_2 *vs.* Fc/Fc^+ [40].

Porphyrin	Metalloporphyrin	Reduction (V)	Metal cation (V)		Metalloporphyrin	Oxidation (V)	
			$(M^{1+}/^{2+})$	$(M^{2+}/^{3+})$			
H_2P36	−2.03	−1.71	–	–	0.44	0.85	1.1
H_2P37	−2.05	−1.7	–	–	0.46	0.87	1.1
Co(II)P36	−1.95	–	−1.44	0.34	0.51	0.75	1.34
Co(II)P37	−1.95	–	−1.44	0.34	0.51	0.78	1.36
Ni(II)P36	–	−1.81	–	–	0.5	0.84	1.29
Ni(II)P37	–	−1.8	–	–	0.5	0.86	1.29
Fe(III)P36	–	−1.6	–	−0.86	0.55	0.98	1.24
Fe(III)P37	–	−1.57	–	−0.84	0.55	0.99	1.26
Mn(III)P36	−2.14	–	–	−0.81	0.63	1.06	1.28
Zn(II)P36	–	−1.92	–	–	0.23	0.5	0.76

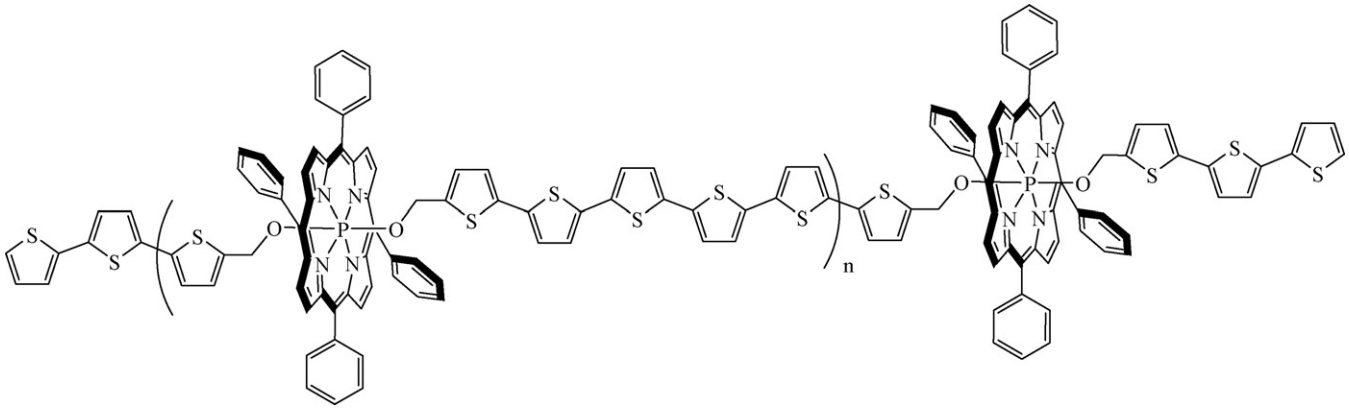

Fig. 26. Polymeric oligothiophene chain of P(V)tetraphenylporphyrins [43].

and terthiophene moieties (λ_{max} = 310, 357 nm respectively) disappeared upon polymerisation with quenching of the fluorescence in the polymers. In addition, the conductivities of **poly-P(V)P42** and **poly-P(V)P43** (Fig. 26) were strongly enhanced upon photoirradiation.

Zinc(II)5,15-bis(4-(2-thienyl)phenyl)-10,20,diphenylporphyrin, **ZnP39** (Fig. 20), failed to form a polymer owing to its low solubility in a range of solvents [42]. Polymeric films of **ZnP40** (Fig. 20) were deposited on an array of electrodes in several solvents by electrochemical oxidation. During the polymerisation process, the polymer film remained electroactive indicating, that the film itself, has enough electrical conductivity to maintain the polymer growth process. An electrode modified with the **poly-ZnP40** exhibits two reversible one-electron porphyrin ring oxidations at 0.78 and 1.06 V *vs.* Ag/AgCl. With potential scan rates of 60–180 mV/s, the potential difference between oxidation and reduction peaks (ΔE_p) was 50–100 mV, indicating the high electroactivity of the porphyrin film. Deposited polymer layers ranging from 5×10^{-10} to 5×10^{-6} mol/cm^2 were reproducible. The synthesised polymer, **poly-ZnP40**, is considered as two isolated redox systems: the porphyrin and the 5,5′bisphenyl-2,2′-bi(3,4-ethylene-dioxy-thiophene). Oxidation of the thienyl subunit occurs at 0.61 V *vs.* Ag/AgCl, cathodic of the porphyrin unit (0.78 and 1.06 V *vs.* Ag/AgCl). Consequently the thienyl subunit in **poly-ZnP40** will only be electroactive after oxidation of the porphyrin ring and as a result the oxidised state of the bithiophene subunit is trapped when the potential scan is reversed. The formation of two distinct redox units in the polymer chain, **poly-ZnP40** (Fig. 27), is believed to be responsible for the observed charge trapping phenomenon, the mechanism for which was supported using model compounds.

Polymerisation of the **ZnP53** and **ZnP54** complexes (Fig. 24) to their respective homopolymers was carried out by electrochemical oxidation [45]. The monomers were also successfully polymerised by chemical oxidation with iron(III) chloride. Cyclic voltammetry on **poly-ZnP53** reveals a zinc porphyrin oxidation in the range 0.6–0.9 V *vs.* Ag/AgCl while oxidation of the thiophene moiety was observed at higher potentials (>1.0 V *vs.* Ag/AgCl). Conductivity measurements of the hydrophobic zinc porphyrinate polymer **poly-ZnP53** on platinum electrodes gave upper values of 6×10^{-3} S/cm. Images of the sodium derivative of the zinc(II) polymer, **poly-ZnP54** (Fig. 28), were recorded by TEM and AFM. The formation of uniform porphyrin wires of up to 2.5 μm in length (*ca.* 1200 monomer units) was confirmed, with a thickness of *ca.* 2 nm corresponding to the width of the porphyrin unit. Light induced charge separations in corresponding acetylene-thiophene connected porphyrins containing other metal ions (Al(III) or Sn(IV)) are currently under investigation by the authors.

4. Dyads/triads containing thienyl porphyrins

4.1. Synthesis

Efficient intramolecular energy transfer from an anthryl donor moiety to a porphyrin acceptor *via* terminally substituted oligothiophene bridging units was reported for the series of compounds **H_2P57**–**H_2P77** (Fig. 29 and Table 8) [48]. *n*-Pentyl groups were incorporated into the oligothiophene chain to increase their solubility.

Freebase mono substituted triphenyl porphyrin oligothiophene dyads, **H_2P78**, **H_2P79** and **H_2P80** were synthesised according to the Lindsey's mixed aldehyde, with coupling to the fullerene unit pro-

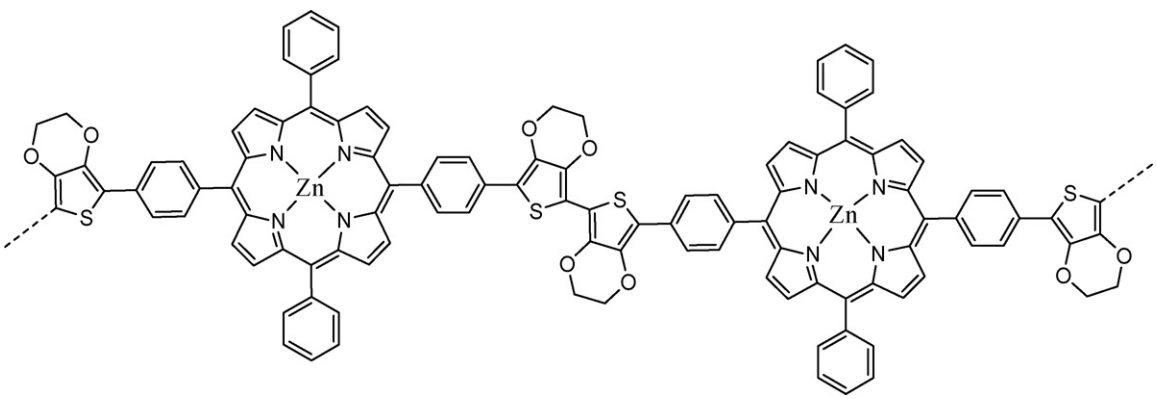

Fig. 27. Poly-ZnP40 [42].

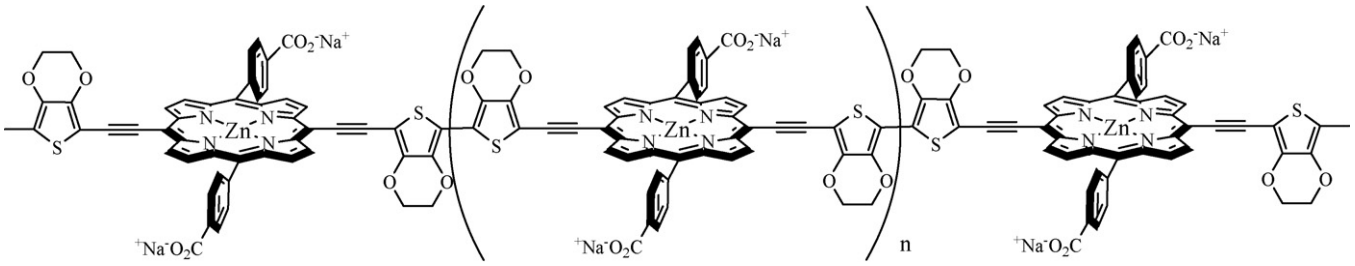

Fig. 28. Poly-ZnP54 [45].

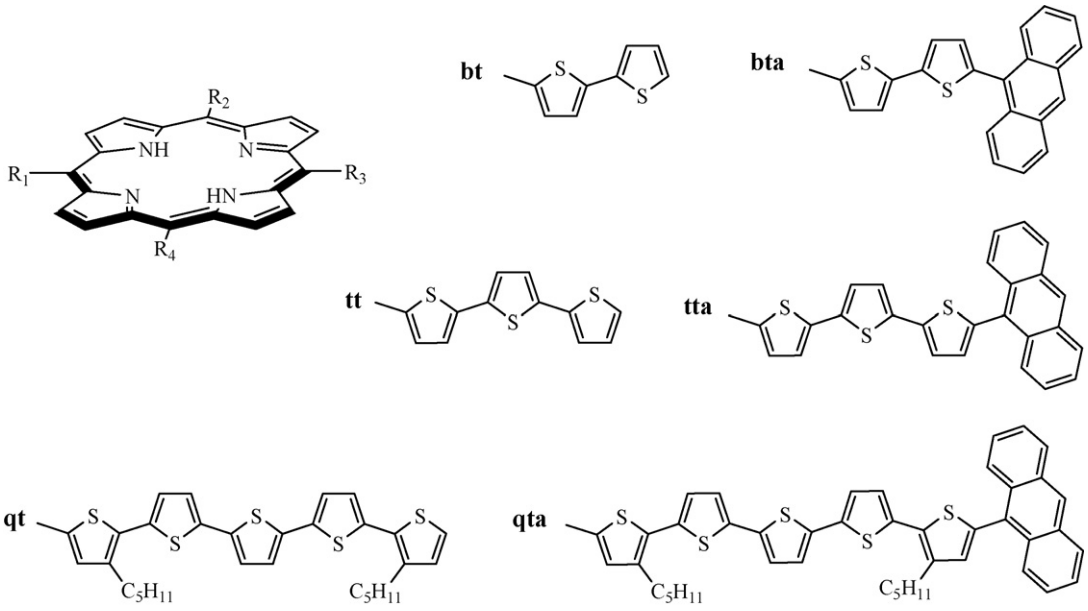

Fig. 29. R groups used to construct porphyrin–oligothiophene–anthracene triads [48].

ducing the triads **H_2P78-C_{60}**, **H_2P79-C_{60}** and **H_2P80-C_{60}** (Fig. 30) in good yield [49].

Hagemann et al. synthesised an "all-in-one" molecular organic solar cell **ZnP81** (Fig. 31) [50]. The convergent synthesis involved 60 steps to produce the dyad that contains all the requisites required for light harvesting, carrier generation, charge separation and transport to external electrodes. Central to the molecule is the zinc porphyrin bisterpyridine ruthenium(II) dyad which has the ability to perform tasks of energy/electron transfer and charge separation. Attached to the porphyrin is a chain of eight 3-hexylthiophene units terminating with an electron donating dimethylaminophenyl group, while a seven-mer hetero-oligophenylvinylene chain terminating with ethyl benzoate is linked to the terpyridine unit. The oligothiophene and oilgophenylvinylene pendant arms were chosen as carrier transporting domains and function as donor and acceptor groups for attraction of the photoinduced charge. The end groups selected can act as possible anchoring units to electrode surfaces.

Table 8
R groups used to make porphyrin–oligothiophene–anthracene dyads [48].

Porphyrin	R_1	R_2	R_3	R_4
P57	bt	bt	bt	bt
P58	tt	tt	tt	tt
P59	bta	*n*-Pentyl	*n*-Pentyl	*n*-Pentyl
P60	bta	*n*-Pentyl	bta	*n*-Pentyl
P61	bta	bta	*n*-Pentyl	*n*-Pentyl
P62	bta	bta	bta	*n*-Pentyl
P63	bta	bta	bta	bta
P64	tta	*n*-Pentyl	*n*-Pentyl	*n*-Pentyl
P65	tta	*n*-Pentyl	tta	*n*-Pentyl
P66	tta	tta	*n*-Pentyl	*n*-Pentyl
P67	tta	tta	tta	*n*-Pentyl
P68	tta	tta	tta	tta
P69	qt	*n*-Pentyl	*n*-Pentyl	*n*-Pentyl
P70	qt	*n*-Pentyl	qt	*n*-Pentyl
P71	qt	qt	*n*-Pentyl	*n*-Pentyl
P72	qt	qt	qt	*n*-Pentyl
P73	qta	*n*-Pentyl	*n*-Pentyl	*n*-Pentyl
P74	qta	*n*-Pentyl	qta	*n*-Pentyl
P75	qta	qta	*n*-Pentyl	*n*-Pentyl
P76	qta	qta	qta	*n*-Pentyl
P77	qta	qta	qta	qta

4.2. Photophysical properties

In spite of the direct attachment of the π-systems of anthracene and/or oligothiophene to the porphyrin macrocycle in **H_2P59**–**H_2P68** and **H_2P73**–**H_2P77** (Fig. 29 and Table 8), the individual molecular subunits observed in the UV–vis spectrum indicate only weak electronic interactions of the π-systems (Table 9) [48]. For all anthracene-oligothiophene-porphyrin molecules, highly selective excitation of the terminal 9-anthryl unit at 258 nm is possible. The supermolecules all possess typical singlet emission from the porphyrin $Q(0,0)^*$ and $Q(0,1)^*$ emission bands. The emission bands are broadened and slightly red shifted compared to **H_2TPP**. Upon excitation at 258 nm, both **H_2P64** and **H_2P67** possess the typical porphyrin emission indicating energy transfer from the anthracene to the porphyrin chromophore. The authors estimate, on the basis of perfect matching of both the absorption

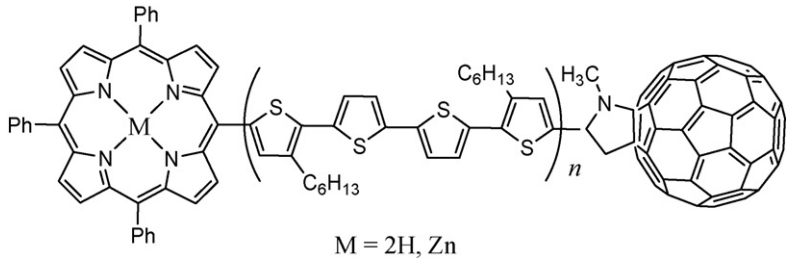

Fig. 30. Porphyrin dyads **H_2P78**: $n = 1$, **H_2P79**: $n = 2$, **H_2P80**: $n = 3$. Porphyrin triads **H_2P78-C_{60}**: $n = 1$, **H_2P79-C_{60}**: $n = 2$, **H_2P80-C_{60}**: $n = 3$ [49].

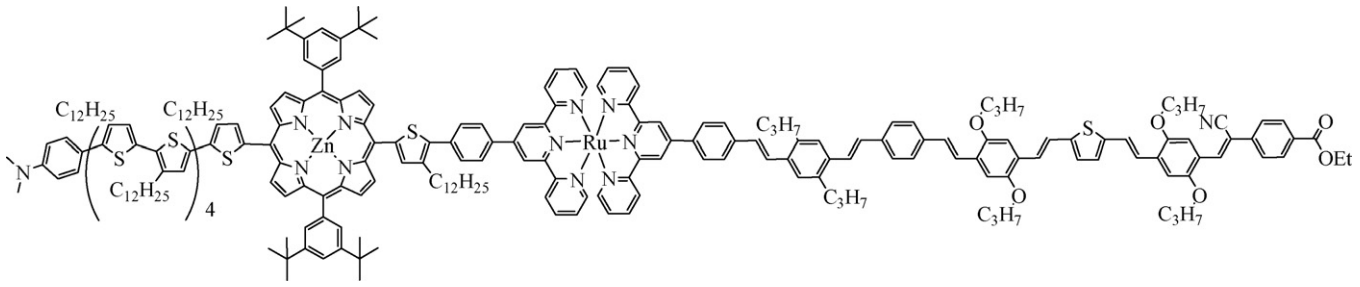

Fig. 31. ZnP81 [50].

and excitation spectra, energy transfer efficiency is ~98%. Both the bithiophene bridged systems **H_2P60** and **H_2P62** gave analogous results. Thus singlet-singlet energy transfer to the porphyrin is the only quenching process for the excited anthracene and oligothiophene moiety. Similar results were found for the dyads **H_2P73**–**H_2P77**, even upon increasing the length of the oligothiophene chain excitation of the intensive anthracene transition leads to typical emission from the porphyrin end group. Neither highly fluorescent anthracene-type nor anthrylquinquethienyl-type emission was detected, thus further confirming energy transfer. The mechanism of energy transfer, i.e. Förster or Dexter, was not clearly identified. The authors do suggest however that due to vibronic coupling, energy is transferred from the anthryl donor to the porphyrin acceptor *via* an intramolecular vibrational relaxation process mediated by the oligothiophene chain. The lifetime of tetrapentylporphyrin is 11.2 ns while the lifetimes of the energy transfer systems decreases to 3.5 ns for **H_2P73**, 3.6 ns for **H_2P64** and 4.4 ns for **H_2P59**. The rate of energy transfer from the anthryl donor to the porphyrin acceptor takes place on a fast timescale resulting in ultrafast emission solely from the porphyrin S_1 excited state with quantum efficiencies of almost 100% for all systems studied.

The absorption spectra of the triads, **H_2P78-C_{60}**–**H_2P80-C_{60}** (Fig. 30), were a super-imposition of all three components, with the porphyrin Soret peak at ~426 nm dominating, thus indicating little interaction among the chromophores in the ground state [49]. However, when the emission spectra of the triads were compared to the respective porphyrin linked oligothiophene dyads, **H_2P78**–**H_2P80**, a reduction in fluorescence was observed in all cases (**P78** triad: 95% decrease, **P79** triad: 46%, **P80** triad: 21%). In all cases quenching was reduced with increasing chain length. The porphyrin fluorescence is efficiently quenched by electron transfer to the fullerene moiety with rate constants for the electron transfer indicating a weak distance dependence of the oligothiophene spacer (Table 10).

In the case of the "all-in-one" complex, **ZnP81** (Fig. 31), the absorption spectrum obtained was dominated by the porphyrin Soret peak at 432 nm which was slightly broadened due to the underlying absorption of the octathiophene moiety (429 nm) [50]. A shoulder at ~480 nm was attributed to the oligophenylenevinylene terminating with a terpyridine moiety, in addition to the observed Q bands at 561 and 608 nm.

The effect of solvent polarity on energy- and electron-transfer in **H_2P78-C_{60}**–**H_2P80-C_{60}** (Fig. 30) and **ZnP78-C_{60}**–**ZnP80-C_{60}** (Fig. 30) was also reported [51]. In toluene, excitation of the freebase porphyrin, $^1H_2P^*$-*n*T-C_{60} (where H_2P represents freebase porphyrins in this class, *n*T represents the number of repeating quaterthiophene units in the oligothiophene spacer and C_{60} represents the fullerene) showed mainly energy transfer (EnT), producing the H_2P-*n*T-$^1C_{60}^*$ moiety. The rate of EnT was inversely proportional to the length of the oligothiophene chain, decreasing with increasing chain length, 3.6×10^9 to 1.4×10^7 s^{-1} respectively upon changing *n*T from $n = 1$ to $n = 3$. In benzonitrile, (PhCN), and *o*-dichlorobenzene, (*o*-DCB), the excited state moiety, $^1H_2P^*$-*n*T-C_{60}, produced the charge separated (CS) species H_2P^+-*n*T-C_{60}^-. The rate constant for this charge separation process decreases with the number of repeating thiophene units in the bridge, indicating that the *n*T moiety acts as a molecular wire. The lifetimes were evaluated by picosecond transient absorption spectroscopy. Lifetimes in the more polar solvent, PhCN, ranged from 1.5 to 2.4 μs, with lifetimes in *o*-DCB ranging from 14 to 27 μs. The longest lifetime

Table 9
Absorption data for some of the porphyrin–oligothiophene–anthracene dyads in *n*-hexane [48].

Porphyrin	Anthracene λ_{max} (nm)	Soret band λ_{max} (nm)	Q bands (nm)
H_2P59	258	421	522, 559, 600, 657
H_2P60/**P61**	258	426	524, 564, 599, 657
H_2P64	258	422	522, 559, 599, 657
H_2P65/**P66**	258	428	525, 565, 600, 659
H_2P67	258	435	526, 573, 598, 663
H_2P73	254	419	519, 555, 601, 659

Table 10
Luminescence data for **P78**–**P80** in benzonitrile (τ_f = fluorescence lifetime, k_{ET} = rate of electron transfer) [49].

Porphyrin dyad	τ_f (s)	Porphyrin triad	k_{ET} (s^{-1})
H_2P78	3.3×10^{-9}	**H_2P78-C_{60}**	5.7×10^9
H_2P79	1.4×10^{-9}	**H_2P79-C_{60}**	6.2×10^8
H_2P80	1.3×10^{-9}	**H_2P80-C_{60}**	2.0×10^8

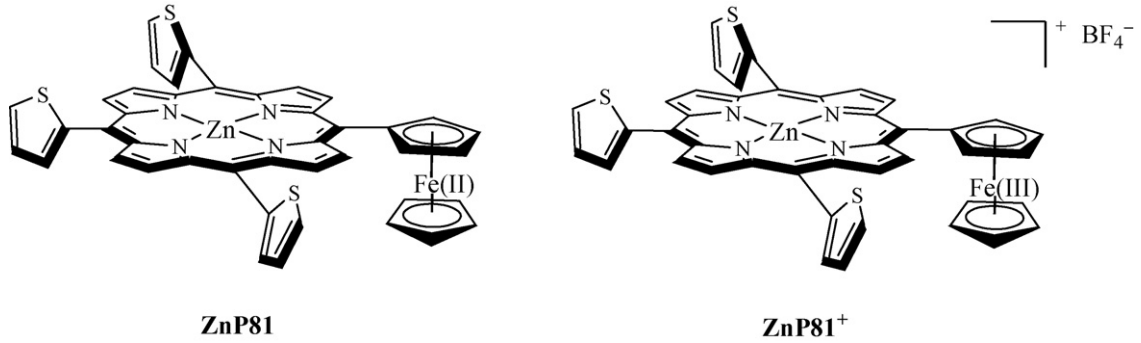

ZnP81 **ZnP81$^+$**

Fig. 32. Zinc(II)tri(thien-2-yl)porphyrin Fe^{II}/Fe^{III} dyads [54].

observed was 27 μs for the H_2P-$2T^+$-C_{60}^- species. The CS process for the zinc porphyrins was examined in three solvents, anisole, *o*-DCB, and PhCN. The authors reported that the CS process is governed by the solvent dielectric constant, and therefore the driving force for the charge separation can be controlled by changing the solvent. The lifetimes for **ZnP78-C$_{60}$** ($n = 1$) and **ZnP79-C$_{60}$** ($n = 2$) were 450 and 910 μs in *o*-DCB, 7.7 and 9.1 μs in anisole and 0.63 and 0.83 μs in PhCN, respectively. The rate of the charge separation process from $^1ZnP^*$ to C_{60} was calculated and the value decreased from 5.0×10^9 for the 1T bridge to $(2.4–9.4) \times 10^8\ s^{-1}$ for the 2T bridge.

Intramolecular charge transfer (ICT) and the related weak distance dependence of the oligothiophene spacer of the porphyrin–oligothiophene–fullerene triads, **H$_2$P78-C$_{60}$–H$_2$P80-C$_{60}$** (Fig. 30), was investigated by quantum chemical methods [52]. Using quantum chemical calculations (time dependent-density functional theory) as well as 2D and 3D real space analysis, the holes and electrons were localised in a specific manner, with two ICT mechanisms possible in the triad. The transition energies and corresponding oscillator strength for the first fifteen excited states were calculated, and the first five studied. Examination of the S_1, S_2 and S_4 states indicated that the electron–hole coherence are mainly between the oligothiophene and fullerene units, with holes localised in the oligothiophene and electrons localised in the fullerene units respectively. Therefore S_1, S_2 and S_4 are ICT states and in these states there is little contribution from the porphyrin unit to ICT. Further assessment of the S_3 and S_5 indicate that they too are ICT states but the electron–hole coherence is mainly between the porphyrin and fullerene units respectively. In these cases the orientation of electron transfer and the majority of the charges transfer from the porphyrin to the fullerene directly, without passing through the oligothiophene spacer. There appears to be little contribution of the thiophene unit to ICT.

Supramolecular systems containing magnesium *meso* tetrakis(thien-2-yl)porphyrin (**MgP1**, Fig. 2) and β-cyclodextrins have been isolated [53]. In a phosphate buffer solution of pH 5.4, **MgP1** formed 1:1 supramolecular systems with β-cyclodextrin and four other modified β-cyclodextrins. The cyclodextrin cavity offers a hydrophobic environment for guest molecules with two of the modified cyclodextrins, dimethoxy-β-cyclodextrin (DM-β-CD) and trimethoxy-β-cyclodextrin (TM-β-CD), substantially increasing this hydrophobic environment. A bathochromic shift and decrease in extinction coefficient in the Soret band of **MgP1**, was observed with formation of the supramolecular system of β-cyclodextrins with **MgP1**. When fluorescent substances move from a polar phase to a non-polar phase, the quantum efficiency of fluorescence increases. An enhancement in emission intensity and shift to shorter wavelength was noted for the DM-β-CD/**MgP1** and TM-β-CD/**MgP1** systems, indicative of the formation of supramolecular systems. These results show that the modified β-cyclodextrins easily form a supramolecular system with **MgP1**.

The on/off switching of porphyrin fluorescence through the use of a ferrocene/ferrocenium (Fc/Fc^+) redox couple has been reported for the zinc(II)tri(thien-2-yl)porphyrin–ferrocene dyad, **ZnP81** (Fig. 32) [54]. The $^1(\pi–\pi^*)$ fluorescence of **ZnP81** is almost completely quenched in comparison to both **ZnP1** (Fig. 2) and **ZnTPP**, with no evidence of the $^3(\pi–\pi^*)$ excited state observed by transient absorption spectroscopy. Attaching the ferrocene moiety at the *meso* position quenches both the $^1\pi–\pi^*$ and $^3\pi–\pi^*$ excited states of the porphyrin ring by rapid electron transfer. The fluorescence in the dyad can be "switched on" by oxidation of ferrocene to the ferrocenium ion. The Fc/Fc^+ redox couple occurs 40 mV positive of the unsubstituted ferrocene and results in the appearance of a low-energy ferrocenium ligand-to-metal charge transfer (LMCT) absorption at ~767 nm. Oxidation of Fe^{II} to Fe^{III}, restores porphyrin emission through preclusion of electron-transfer. The relative fluorescence quantum yield for **ZnP81$^+$** is 71% with respect to **ZnP1** (the minor decrease in fluorescence is attributed to the quenching processes of intersystem crossing of the porphyrin $^1(\pi–\pi^*)$ excited state to the new LMCT state and energy transfer quenching by the ferrocenium unit). Transient absorption spectroscopy of the **ZnP81$^+$** dyad produced transient signals indicative of the $^3(\pi–\pi^*)$ triplet excited state (Fig. 33). A triplet lifetime of 20 μs was obtained for **ZnP81$^+$**, a reduction of 50% in comparison to **ZnP1** (40 μs). Similarly, the $^1(\pi–\pi^*)$ singlet excited state lifetime of 0.31 ns observed for **ZnP81$^+$**, is shorter than that of **ZnP1** (0.56 ns).

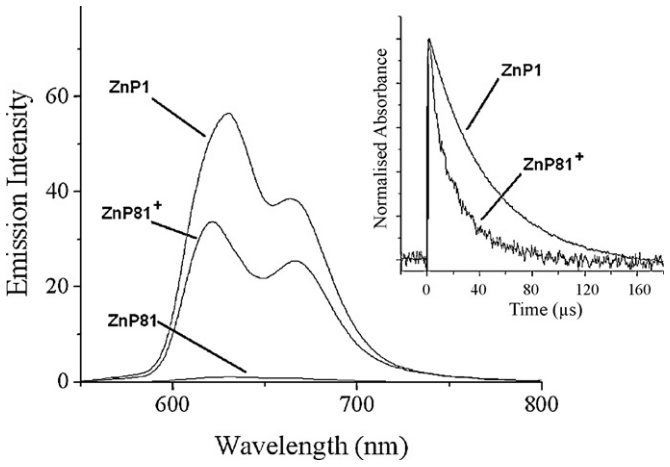

Fig. 33. Fluorescence spectra of **ZnP1**, **ZnP81** and **ZnP81$^+$** in ethanol. (Inset) Normalised transient absorption decay traces of **ZnP1** and **ZnP81$^+$** at 490 nm (λ_{exc} 532 nm; 1 atm of argon, in ethanol) [54].
Reproduced from reference [54] with permission of the copyright holders.

5. Dithienylethene switches tethered to porphyrin macrocycles

5.1. Synthesis and photophysical properties

A photochromic hybrid **H_2P82** (Fig. 34) containing porphyrin macrocycles tethered to the ends of 1,2-bis(thien-3-yl)cyclopentene has been reported [55]. The absorption spectrum of the hybrid molecule is the sum of the individual components (the phenyl functionalised photochrome and the porphyrin) thus indicating little or no change in the ground state of either chromophore upon covalent linking. Irradiation at 313 nm produces the "*closed*" form of the switch, with an immediate increase in the absorption bands in the visible region (500–625 nm). Irradiation of the "*closed*" form at wavelengths greater than 480 nm results in regeneration of the original absorption spectrum thus signifying reversal to the "*open*" form. In the "*open*" form, excitation of the porphyrin at 430 nm produces a strong emission centred 655 nm. However following photocyclisation of the switch to the "*closed*" form, the porphyrin unit is non-fluorescent. Therefore the luminescence properties of the porphyrin greatly depend on the state of the dithienylethene (DTE) moiety. As the 1,2-(dithienyl)cyclopentene fragment of **H_2P82** is transparent in the Soret band region, the porphyrin moiety can be selectively irradiated at 420 nm. Continuous irradiation of the "*closed*" hybrid (**H_2P82**) at 430 nm resulted in an increase (~45%) in the emission with a concomitant decrease in the absorption spectrum (500–625 nm). It is likely that partial ring opening is due to the porphyrin moiety absorbing at 430 nm and channelling of the excited state energy towards the photochromic centre.

A dithienylethene (DTE) -tetraphenylporphyrin (P) -fullerene (C_{60}) triad, **DTE-H_2P83-C_{60}** (Fig. 35), which may act as an electron transfer switch was reported by Gust and co-workers [56]. When the DTE is in its "*open*" configuration, in **DTE-H_2P83-C_{60}**, the porphyrin excited state donates an electron to C_{60} with a quantum yield of unity, thus forming the CS species, DTE-$P^{\bullet+}$-$C_{60}{}^{\bullet-}$. The dyad **DTE-H_2P83** consisting of the DTE and porphyrin units (Fig. 35) was also synthesised, so as to investigate the affect of the DTE moiety on the excited state dynamics of the porphyrin chromophore. UV light (360 nm) converts **DTE-H_2P83** to the "*closed*" form, with visible light (600 nm) converting DTE to the "*open*" form. The "*open*" form of **DTE-H_2P83** displays typical porphyrin emission, with the porphyrin emission strongly quenched in the "*closed*" form. Irradiation of the triad (**DTE-H_2P83-C_{60}**) at 360 nm converts the DTE moiety to its "*closed*" configuration. In this form the porphyrin excited state is quenched by singlet-singlet energy transfer to the "*closed*" DTE moiety in ~2 ps, with electron transfer to the fullerene acceptor strongly precluded. Transient absorption spectroscopy confirms this, as no significant fullerene radical anion absorption was observed in the region from 930 to 1050 nm.

Shin and Park have reported the synthesis and photophysical properties of a dithienylethene moiety linked between two porphyrins (**H_2P84** and **ZnP84**, Fig. 36) [57]. The absorption spectra of **H_2P84** and **ZnP84** is the summation of the individual parts (dithienylcyclopentene λ_{max} = 275 nm and freebase porphyrin λ_{max} = 419 nm, zinc porphyrin λ_{max} = 421 nm). Following excitation at 420 nm, the fluorescence spectra of **H_2P84** and **ZnP84** display emission bands at 652, 718 nm and 599, 647 nm respectively. Fluorescence quantum yields of 0.09 for **H_2P84** and 0.06 for **ZnP84** were similar to those of **ZnTPP** (0.09). The absorption and fluorescence data indicate that there is little communication between the DTE and porphyrin units. UV irradiation (275 nm) of **ZnP84** yields the "*open*" form and the "*closed*" form is regenerated following irradiation at 600 nm. The "*open*" form of the ZnP-DTE-ZnP binds with 4,4′-bipyridyl like a tweezers, while the "*closed*" form, because of its structural rigidity and wider interporphyin distance cannot. Axial ligation of 4,4′-bipyridyl occurs, presumably due to flexibility of the porphyrin rings. Following axial coordination of the bidentate ligand in **ZnP84** the Soret and Q bands (λ_{max} Q bands = 551 and 591 nm) are bathochromically shifted (Soret band λ_{max} = 429 nm, Q bands = 564 and 604 nm). A 1:1 stiochiometry between **ZnP84** and 4,4′-bipyridyl was estimated from Jobs plot. Complexation with the bipyridyl unit results in the quenching of the **ZnP84** fluorescence. As the formation constants (determined from absorption and fluorescence studies) for the complex between **ZnP84** and 4,4′-bipyridyl were considerably higher than those for the porphyrin monomer, the authors suggest that binding of the

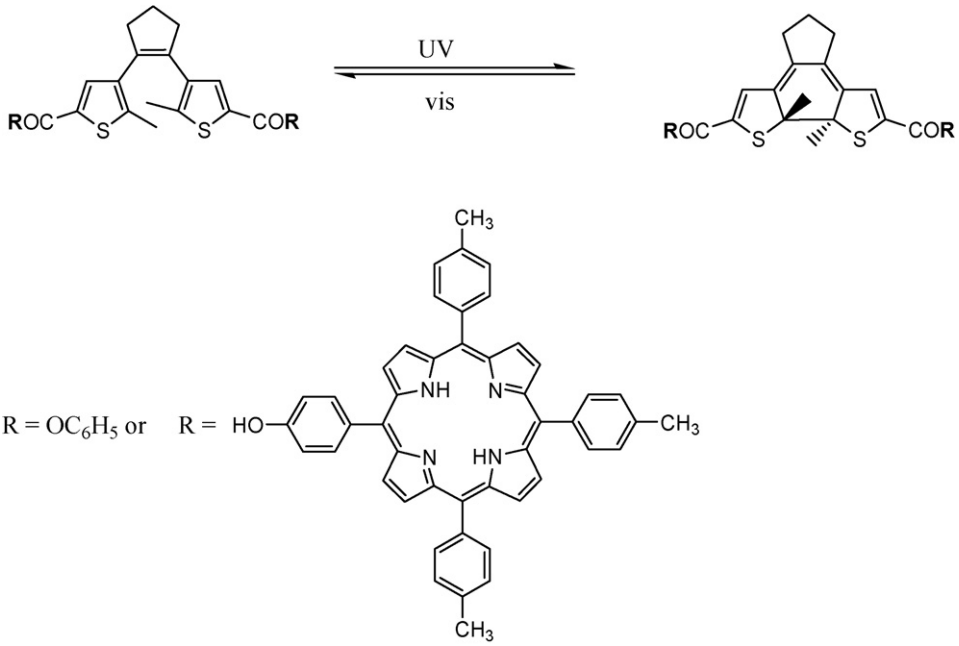

Fig. 34. Photochromic porphyrin hybrid, **H_2P82** [55].

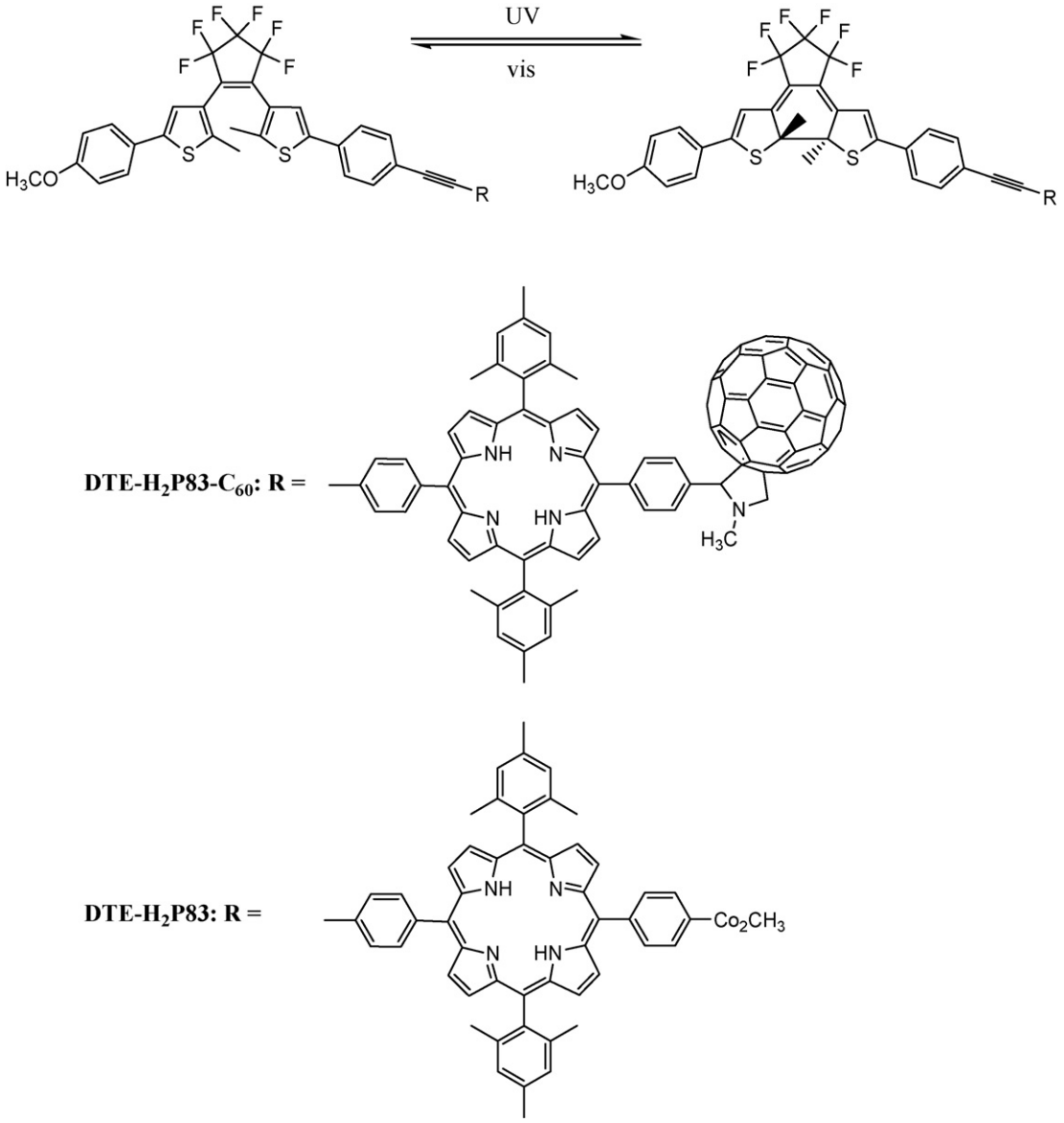

Fig. 35. DTE switches containing porphyrin units [56].

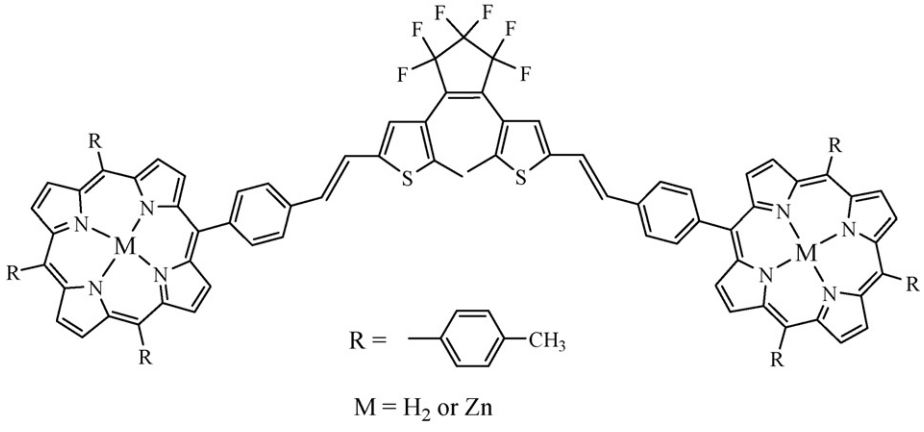

Fig. 36. DTE linked porphyrin, **P84** [57].

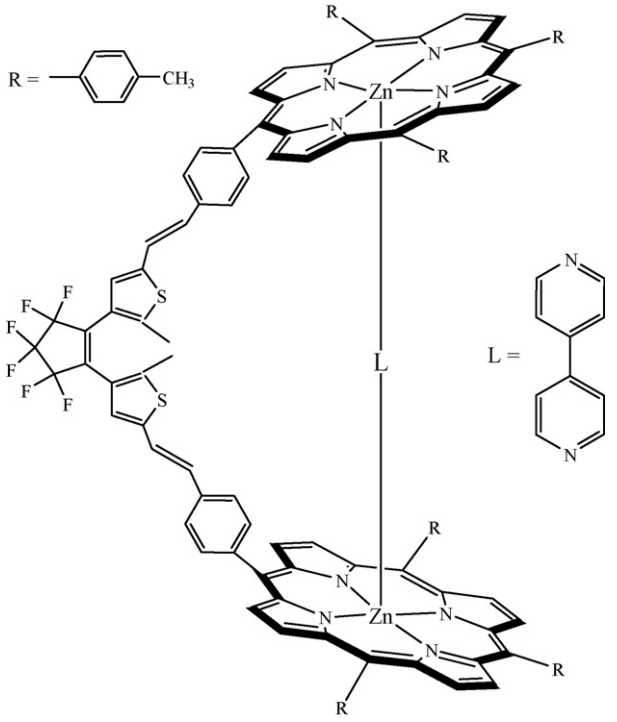

Fig. 37. Sandwich type structure of **ZnP84** with 4,4′-bipyridyl [57].

bipyridyl ligand occurs between the two porphyrin centres, thus yielding a sandwich type compound as shown in Fig. 37.

Electronic differences are most dramatically manifested by how molecules react or interact with others and this was the focus of another paper based on DTE switches [58]. The photoregulation of reactivity is shown by the "*open*" and "*closed*" forms of the DTE isomers of the mono-alkylated bis(pyridine) (Fig. 38). In the "*open*" configuration the isomer lacks co-planarity and linear π-conjugation, resulting in two pendant pyridine rings electronically insulated from one another. The nucleophilic pyridine in these systems does not sense the electronic pull of the electron deficient pyridinium cation. However photocyclisation (365 nm) to the "*closed*" configuration brings about linear π-conjugation in the molecular backbone and the two formerly independent pyridine rings are now electronically coupled. To demonstrate the difference in Lewis basicity in the "*open*" and "*closed*" form in the DTE switch, axial coordination of pyridine to a ruthenium porphyrin to produce **P85** was monitored. A solution containing only the "*open*" form of the DTE compound was irradiated (λ = 365 nm) until a 50:50 mixture of ring-*open* and ring-*closed* isomers were present. Treatment of this mixture with the metalloporphyrin (Fig. 38) resulted in partial coordination of the porphyrin complex to the DTE switch (shown by ^{1}H NMR, as N–Ru binding is slow). Results indicated that the "*open*" isomer binds a higher amount (1.5 times) of the porphyrin macrocycle compared to the "*closed*" isomer, which suggests that the ring-*open* isomer is a more effective ligand.

6. Applications

As previously mentioned at the beginning of this review the various applications of porphyrins are numerous, including such areas such as catalysis, medicinal, new materials, solar cell devices and so forth. In this section we have focused on specific applications of the thienyl porphyrins that have appeared in the literature to date.

The **poly-FeP2** (Fig. 15) modified electrode is the first all-synthetic electrochemical sensor for the superoxide anion radical ($O_2^{\bullet -}$) due to its efficient electrocatalytic oxidation of $O_2^{\bullet -}$ to O_2. To mimic the iron centre of cytochrome-*c*, an iron(III) porphyrin modified electrode was developed by Yuasa et al. [59]. The **[Fe(im)P2]$^+$Br$^-$** electrode was applied to detect $O_2^{\bullet -}$ and results indicated that $O_2^{\bullet -}$ was catalytically oxidised at the modified electrode. The presence of the imidazole ligand enables the oxidation of $O_2^{\bullet -}$ by an outer sphere process, comparable to cytochrome-

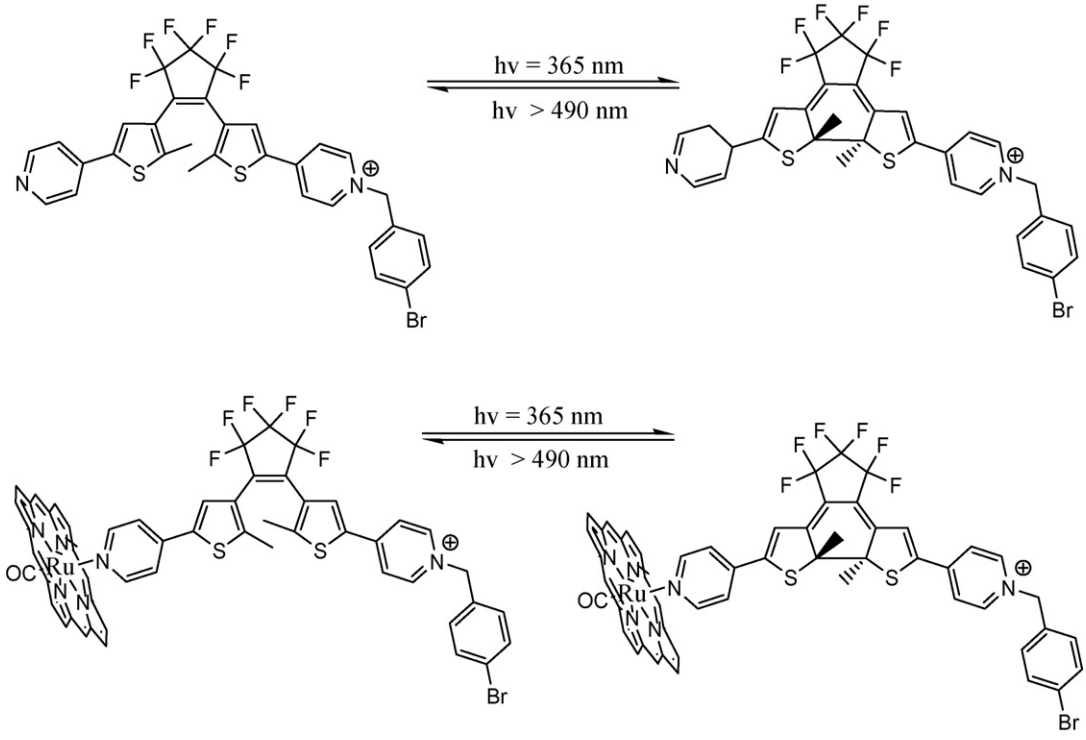

Fig. 38. Formation of **P85** by axial coordination of a DTE switch with the porphyrin [58].

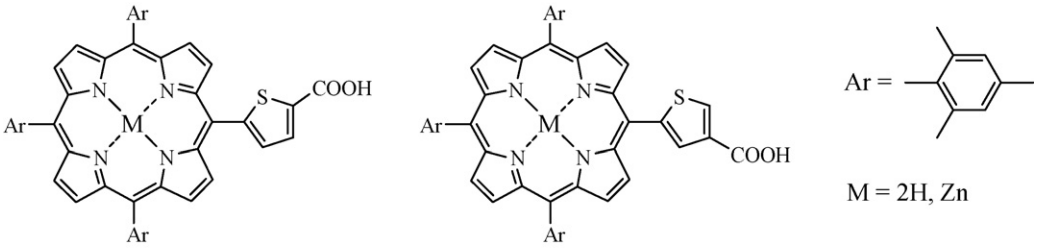

P86 **P87**

Fig. 39. Monosubstituted porphyrins **P86** and **P87**.

c mediated $O_2^{\bullet -}$ oxidation, with current density of the electrode reported as *ca.* 3.6×10^2 nA μM^{-1} cm^{-2}. The sensitivity of the system toward $O_2^{\bullet -}$ is 50 times higher than that obtained in a previous study using a modified cytochrome *c*–Au electrode (typically ~6 nA μM^{-1} cm^{-2}) [60].

Electrochemical studies have shown that the band gap in thienyl porphyrins **ZnP8**–**ZnP13** (Fig. 4) can be controlled by varying the number of thienyl substituents on the macrocyclic ring and by the nature of the thienyl substituent (i.e. thiophene *vs.* bromothiophene) [21]. The reduction in band gap previously discussed follows the order **ZnP9** (2.02 eV) < **ZnP13** (2.02 eV) < **ZnP12** (2.04 eV) < **ZnP11** (2.06 eV) < **ZnTPP** (2.09 eV). Hence, through molecular design the application of thienylporphyrins in optoelectronic devices becomes a real possibility, e.g. energy alignment in photovoltaic and dye sensitised solar cell devices.

The non-linear optical properties *viz.* the molecular first hyperpolarisability, β (Table 3) was evaluated using femtosecond hyper-Rayleigh scattering (fs-HRS) pulsed laser measurements for a range of thienyl systems [25]. Exceptionally large dynamic hyperpolarisability values in the range 670–4350 × 10^{-30} esu were obtained at 1300 nm incident irradiation. The value of 4350 × 10^{-30} esu, obtained for **ZnP18** (Fig. 6), is the largest β_{1300} value, measured at 1300 nm incident radiation, for an uncharged chromophore. Using the same technique the molecular first hyperpolarisability values for **ZnP22**–**ZnP25** (Fig. 6) were determined. **ZnP22**'s formyl group drives a blue shift in the Q band (λ_{max} = 676 nm), whereas **ZnP23**'s strong dicyanovinyl acceptor causes a red shift in the Q band (λ_{max} = 698 nm) relative to **ZnP19** (λ_{max} = 685 nm). Compounds **ZnP24** and **ZnP25** are analogues of **ZnP19** in which there is an inversion of charge-transfer direction. **ZnP25** shows diminished excited-state structural heterogeneity relative to **ZnP19** and **ZnP24**, caused by the planarity of the conjugated carbazolyl unit. As a result both **ZnP24** and **ZnP25** β_{1300} values (Table 3) exceed that measured for **ZnP19**, but interestingly, **ZnP25** exceeds that of **ZnP19** and **ZnP24** by approximately 2-fold. These enhanced hyperpolarisabilities, with respect to **ZnP19**, indicate that further improvements in the already large magnitude β_{1300} values within the porphyrin–oligothiophene based chromophores should be possible.

The anthracene donor in porphyrins **H_2P59**–**H_2P68** and **H_2P73**–**H_2P77** (Fig. 29 and Table 8) have highly selective UV antenna that can be excited with up to 90% efficiency [48]. After excitation quantitative intramolecular energy transfer (>98%) from the anthracene through the oligothiophene unit to the emitting porphyrin acceptor was shown. In previous studies by the authors, where polyene bridges were used, radiationless deactivation of the excitation energy through the conjugated chain and quenching of the acceptor emission was observed [61]. The results based on the oligothiophene systems suggest that oligothiophenes are far superior with regard to mediating energy transfer and show greater potential for application in molecular electronics. The anthryloligothiophene moiety functions as an efficient light harvesting antenna system, which substantially increases the absorption cross-section in the UV range with respect to the unsubstituted porphyrins.

Mono substituted porphyrins (**ZnP86** and **ZnP87**, Fig. 39) with *meso* 5-membered heteroaromatic groups were designed to evaluate the effects of the spacer on mesoporous TiO_2 nanoparticle films [13]. The carboxylic group ensured a single point of attachment to the surface. The three remaining mesityl *meso* substituents possess large steric hindrance, reducing aggregation of the porphyrin molecules. Porphyrin-modified ITO/TiO_2 electrodes were produced by adsorbing the porphyrin onto the prepared ITO/TiO_2 electrode. **ZnP86** adsorbed quickly and formed a densely packed porphyrin monolayer whereas **ZnP87** adsorbed at a slower rate and formed a loosely packed monolayer. Total amounts of porphyrin adsorbed onto the TiO_2 film were calculated as $\Gamma = 2.0 \times 10^{-11}$ mol cm^{-2} for **ZnP86** and $\Gamma = 1.2 \times 10^{-10}$ mol cm^{-2} for **ZnP87**. The calculated porphyrin density value together with the tilt of the molecules is responsible for the packing on the surface. **ZnP87** is tilted almost parallel to the TiO_2 surface and adsorbs in a tightly packed monolayer whereas **ZnP86**'s horizontal orientation of the acid group results in a loosely packed monolayer. The ITO/TiO_2/porphyrin dye sensitised solar cell device sensitised with **ZnP86**, possesses high photovoltaic properties with a maximum incident photon-to-current-efficiency (IPCE) of 65% in the region of the Soret absorption and a maximum power conversion efficiency (η_{max}) of 3.1%. Values of $IPCE_{max}$ = 34% and η_{max} = 2.0% were obtained for **ZnP87**. The higher effectiveness of **ZnP86** is attributed to the additional electron-transfer pathway through specific interaction between the sulphur atom in the bridge and the TiO_2 surface.

A copolymer of **H_2P88** and terthiophene, **poly-H_2P88** (Fig. 40), was the basis for a novel photoelectrochemical cell [62]. The use of a porphyrin co-polymer improved the light harvesting capabilities of a previously synthesised polythiophene-based photovoltaic device. Scanning electron microscopy of **poly-H_2P88** showed an open porous morphology (Fig. 41) which is beneficial for photovoltaics due to the larger surface area. A series of porphyrin to terthiophene monomer mole ratios were also investigated and equimolar amounts of each monomer gave the best energy conversion results. This photovoltaic device had an energy conversion efficiency of 0.09%. An additional increase (0.06–0.12%) was also observed in the efficiency of the copolymer after soaking in a zinc(II) solution due to metallation of *ca.* 25% of the porphyrin units on the polymer backbone.

Friedlein et al. reported the self-assembly of supramolecular columns of large polycyclicaromatic hydrocarbons and thienyl porphyrins [63]. **ZnP8** (Fig. 4) was used for this "bottom-up" synthetic strategy of a highly ordered nanostructure at a molybdenum disulfide (MoS_2) surface. Bromination of the peripheral 5′-position of the thiophene increased solubility and facilitated the self assembly of the columnar nanostructures in solution.

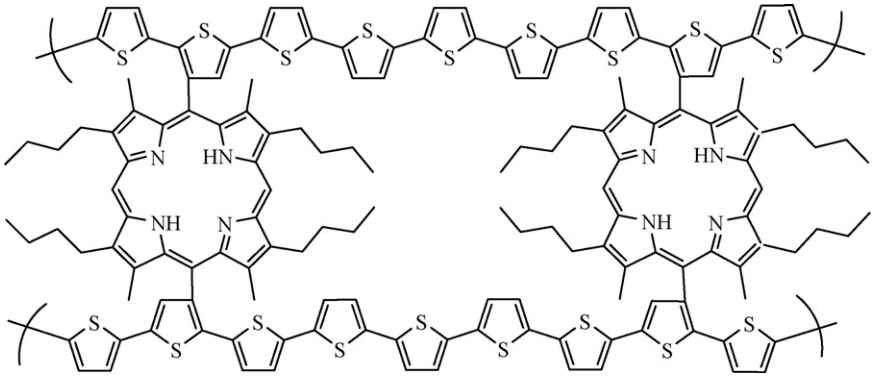

Fig. 40. Poly-H_2P88 [62].

Tapping-mode scanning force microscopy (TM-SFM) indicated the film was flat (10 nm thick, ±2 nm) and the surface was completely covered. Photoelectron spectroscopy was used to investigate the alignment of the nanostructures on the surface. Spectral changes observed upon annealing were attributed to increased structural order in the columnar arrangements. Cone-like photoelectron emission around the molecular axis (typical for π-electronic states of discotic molecules) indicates a flat orientation of the porphyrin rings, face to face with the surface substrate. The nanostructures display anisotropic conducting pathways with long coherence length. Ordered films of porphyrins with functional side groups (e.g. thiophene) are good candidates for (opto-)electronic applications where fast charge separation and transport are required. The alignment of the columns is also ideal for solar cell applications.

Hagemann et al. synthesised the multi-domain macrocycle **ZnP81** (Fig. 31), with all the photophysical and electronic functionalities necessary for a solar cell in one molecule [50]. The most promising materials reported to date for organic solar cells are based on simple polymers and use bulk heterojunction devices with the electron acceptor [6,6]-phenyl-C_{61}-butyric acid methyl ester (PCBM). Hagemann et al. used such systems for comparison purposes. In the case of **ZnP81** a photovoltaic device was created and compared to devices constructed from oligomeric 3-hexythiophene. Values of 0.18 V for open circuit voltage, 0.0044 mAcm^{-2} for short circuit current, 29% fill factor and 0.000081% for efficiency were obtained. No dark recitication was observed. This porphyrin assembly did not compare well, to the model systems, being 100 times less efficient than the device based on the reference 3-hexylthiophene oligomer and 1000 times worse than PBCM. The experiments show that while the molecule efficiently converts the energy internally, it is inefficient at generating and separating charge carriers.

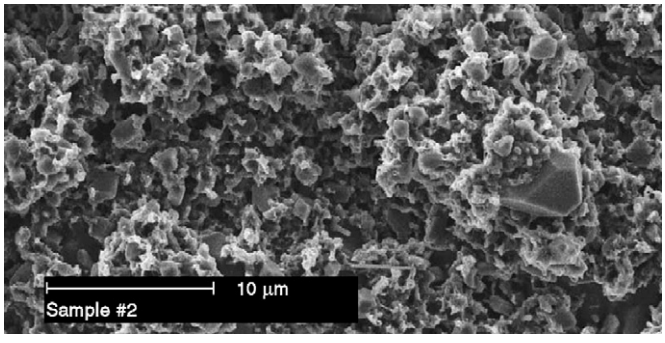

Fig. 41. Scanning electron micrograph of **poly-H_2P88** [62].
Reproduced from reference [62] with permission of the copyright holders.

7. Conclusion

Since their discovery, thienyl porphyrins have consistently been investigated to determine the source of their unique properties while new synthetic methods are continuously developing to generate totally or partially conjugated macrocycles with thienyl moieties. Characterised by their unique absorbance and fluorescence spectra, communication between thienyl porphyrins and other organic moieties has inspired the production of copious assemblies. Control of their fluorescence properties finds use in the generation of molecular switches, while their light harvesting abilities makes them model candidates in synthetic photochemical cells.

The co-planar arrangement of the thienyl group to the porphyrin macrocycle allows an extension of the π-system through conjugation. This imparts rich electrochemical properties, which makes these macrocycles ideal for use as building blocks in linear porphyrin arrays as well as supramolecular assemblies. Facile polymerisation *via* the thienyl subunits by chemical or electrochemical means produces bis- or oligo-porphyrin linked polymers containing thienyl bridges as a conjugating molecular wire. These thienyl porphyrin polymers exhibit higher electrochemical stability than many other porphyrin polymers reported to date. Thienyl porphyrin modified electrodes display high conductivity, ideal for the production of organic conductors. Hybrid materials containing thienyl porphyrins that show the dual properties of a conducting and redox polymer can be used in sensor design. Supramolecular donor–acceptor chromophores have shown interesting linear and nonlinear properties and display high relatively IPCE values necessary for efficient solar cells operation. Control of energy and electron transfer, necessary for effective photovoltaic cells has also been demonstrated in many multidomain assemblies. The work involving thienyl porphyrins to date has produced many fascinating results and their rich photophysical, photochemical and electrochemical properties will undoubtedly continue to stimulate research in many fields.

References

[1] G. Simonneaux, P. Le Maux, Coord. Chem. Rev. 43 (2002) 228.
[2] K. Lang, J. Mosinger, D.M. Wagnerová, Coord. Chem. Rev. 248 (2004) 321.
[3] M. Calvete, G. Ying Yang, M. Hanack, Synth. Met. 141 (2003) 231.
[4] (a) K.M. Kadish, K.M. Smith, R. Guilard (Eds.), The Porphyrin Handbook, vol. 8, Academic Press, Boston, 2000;
(b) K.M. Kadish, K.M. Smith, R. Guilard (Eds.), The Porphyrin Handbook, vol. 18, Academic Press, Boston, 2003.
[5] (a) K.M. Kadish, K.M. Smith, R. Guilard (Eds.), The Porphyrin Handbook, vol. 2, Academic Press, Boston, 2000;
(b) K.M. Kadish, K.M. Smith, R. Guilard (Eds.), The Porphyrin Handbook, vol. 9, Academic Press, Boston, 2000;
(c) K.M. Kadish, K.M. Smith, R. Guilard (Eds.), The Porphyrin Handbook, vol. 14, Academic Press, Boston, 2003.

[6] A. Treibs, N. Haeberie, Justus Liebigs Ann. Chem. 718 (1968) 183.
[7] M.A. Torréns, T.K. Straub, L.M. Epstein, J. Am. Chem. Soc. 94 (1972) 4160.
[8] P. Bhyrappa, P. Bhavana, Chem. Phys. Lett. 349 (2001) 399.
[9] J.S. Lindsey, I.C. Schreiman, H.C. Hsu, P. Kearney, A.M. Marguerettaz, J. Org. Chem. 52 (1987) 827.
[10] N. Ono, H. Miyagawa, T. Ueta, T. Ogawa, H. Tani, J. Chem. Soc., Perkin Trans. 1 (1998) 1595.
[11] C.J. Medforth, R.E. Haddad, C.M. Muzzi, N.R. Dooley, L. Jaquinod, D.C. Shyr, D.J. Nurco, M.M. Olmstead, K.M. Smith, J.-G. Ma, J.A. Shelnutt, Inorg. Chem. 42 (2003) 2227.
[12] G.E. Collis, W.M. Campbell, D.L. Officer, A.K. Burrell, Org. Biomol. Chem. 3 (2005) 2075.
[13] C.-S. Duanmu, Z.-P. Chen, X.-S. Yu, X. Zhou, Chin. J. Chem. 22 (2004) 779.
[14] S. Eu, S. Hayashi, T. Umeyama, A. Oguro, M. Kawasaki, N. Kadota, Y. Matano, H. Imahori, J. Phys. Chem. C 111 (2007) 3528.
[15] Y.L.S.-T. Arminger, T.D. Lash, J. Heterocycl. Chem. 29 (1992) 523.
[16] C.O. Paul-Roth, J. Letessier, S. Juillard, G. Simonneaux, T. Roisnel, J. Rault-Berthelot, J. Mol. Struct. 872 (2008) 105.
[17] R.P. Bonar-Law, J. Org. Chem. 61 (1996) 3623.
[18] D.F. Shi, R.T. Wheelhouse, Tetrahedron Lett. 43 (2002) 9341.
[19] J.S. Lindsey, J.N. Woodford, Inorg. Chem. 34 (1995) 1063.
[20] R. Friedlein, X. Crispin, W. Osikowicz, S. Braun, M.P. de Jong, C.D. Simpson, M.D. Watson, F. von Kieseritzky, P. Samorí, S.K.M. Jönsson, M. Fahlman, F. Jäckel, J.P. Rabe, J. Hellberg, K. Müllen, W.R. Salaneck, Synth. Met. 147 (2004) 79.
[21] J. Rochford, S. Botchway, J.J. McGarvey, A.D. Rooney, M.T. Pryce, J. Phys. Chem. 112 (2008) 11611.
[22] T. Yamamoto, N. Fukushima, H. Nakjima, T. Maruyama, I. Yamaguchi, Macromolecules 33 (2000) 5988.
[23] M. Yuasa, K. Oyaizu, A. Yamaguchi, M. Ishikawa, K. Eguchi, T. Kobayashi, Y. Toyoda, S. Tsutsui, Polym. Adv. Technol. 16 (2005) 616.
[24] T. Shimidzu, H. Segawa, F. Wu, N. Nakayama, J. Photochem. Photobiol. A: Chem. 92 (1995) 121.
[25] (a) T.-G. Zhang, Y. Zhao, I. Asselberghs, A. Persoons, K. Clays, M.J. Therin, J. Am. Chem. Soc. 127 (2005) 9710;
(b) T.-G. Zhang, Y. Zhao, K. Song, I. Asselberghs, A. Persoons, K. Clays, M.J. Therin, Inorg. Chem. 45 (2006) 9703.
[26] P. Bhavana, B. Verghese, P. Bhyrappa, Acta Crystallogr. C57 (2004) 252.
[27] Y. Diskin-Posner, S. Balasubramanian, G.K. Patra, I. Goldberg, Acta Crystallogr. E57 (2001) m346.
[28] P. Bhyrappa, M. Sankar, B. Varghese, P. Bhavana, J. Chem. Sci. 118 (2006) 393.
[29] M. Bellizzi, P.C.D. Foss, R. Pelto, G. Crundwell, C. Brückner, J.B. Updegraff III, M. Zeller, A.D. Hunter, Z. Kristallogr. 219 (2004) 129.
[30] X. Sun, J. Zhang, B. He, J. Photochem. Photobiol. A: Chem. 172 (2005) 283.
[31] C. Brückner, P.C.D. Foss, J.O. Sullivan, R. Pelto, M. Zeller, R.R. Birge, G. Crundwell, Phys. Chem. Chem. Phys. 8 (2006) 2402.
[32] J. Rochford, Steady state and laser flash photolysis studies of ferrocenyl group VI Fischer-carbenes and metalloporphyrins, Thesis (Ph.D.), Dublin City University, 2004.
[33] S. Okada, H. Segawa, J. Am. Chem. Soc. 125 (2003) 2792.
[34] (a) K.M. Kadish, E. Van Caemelbecke, G. Royal, in: K.M. Kadish, K.M. Smith, R. Guilard (Eds.), The Porphyrin Handbook, vol. 8, Academic Press, Boston, 2000 (Chapter 55);
(b) M.O. Senge, in: K.M. Kadish, K.M. Smith, R. Guilard (Eds.), The Porphyrin Handbook, vol. 1, Academic Press, Boston, 2000, p. 239.
[35] C. Paul-Roth, J. Rault-Berthelot, G. Simonneaux, C. Poriel, M. Abdalilah, J. Ltessier, J. Electroanal. Chem. 597 (2006) 19.
[36] H. Maruyama, H. Sewaga, S. Sotoda, T. Sato, N. Kosai, S. Sagisaka, T. Shimidzu, K. Tanaka, Synth. Met. 96 (1998) 141.
[37] M.J. Crossley, J.K. Prashar, Tetrahedron Lett. 38 (1997) 6751.
[38] N. Ono, H. Hironaga, K. Ono, S. Kaneko, T. Murashina, T. Ueda, C. Tsukamura, T. Ogawa, J. Chem. Soc., Perkin Trans. 1 (1996) 417.
[39] A. Rohrer, R. Ocampo, H.J. Callot, Bull. Soc. Chim. Fr. 134 (1997) 689.
[40] M. Schaferling, P. Bauerle, J. Mater. Chem. 14 (2004) 1132.
[41] (a) B. Ballarin, S. Masiero, R. Seeber, D. Tonelli, J. Electroanal. Chem. 449 (1998) 173;
(b) B. Ballarin, R. Seeber, L. Tassi, D. Tonelli, Synth. Met. 114 (2000) 279.
[42] G. Li, S. Bhosale, S. Tao, R. Guo, S. Bhosale, F. Li, Y. Zhang, T. Wang, J.-H. Fuhrhop, Polymer 46 (2005) 5299.
[43] (a) H. Segawa, N. Nakayama, T. Shimidzu, J. Chem. Soc., Chem. Commun. (1992) 784;
(b) H. Segawa, N. Nakayama, F. Wu, T. Shimidzu, Synth. Met. 966 (1993) 55.
[44] (a) P. Janvier, J.-Y. Lequestel, B. Illien, S. Suresh, E. Blart, J.-P. Quintard, F. Odobel, Int. J. Quantum Chem. 84 (2001) 259;
(b) F. Odobel, S. Suresh, E. Blart, Y. Nicolas, J.-P. Quintard, P. Janvier, J.-Y. Le Questel, B. Illien, D. Rondeau, P. Richomme, T. Häupl, S. Wallin, L. Hammarström, Chem. Eur. J. 8 (2002) 3027.
[45] G. Li, T. Wang, A. Schulz, S. Bhosale, M. Lauer, P. Espindola, J. Heinze, J.-H. Fuhrhop, Chem. Commun. (2004) 552.
[46] M.-C. Kuo, L.-A. Li, W.-N. Yen, S.-S. Lo, C.-W. Lee, C.-Y. Yeh, Dalton Trans. (2007) 1433.
[47] D.P. Arnold, D.A. James, C.H.L. Kennard, G. Smith, J. Chem. Soc., Chem. Commun. (1994) 2131.
[48] (a) F. Wurthner, M.S. Vollmer, F. Effenberger, P. Emele, D.U. Meyer, H. Port, H.C. Wolf, J. Am. Chem. Soc. 117 (1995) 8090;
(b) M.S. Vollmer, F. Wurthner, F. Effenberger, P. Emele, D.U. Meyer, T. Stumpfig, H. Port, H.C. Wolf, Chem. Eur. J. 4 (1998) 260.
[49] J. Ikemoto, K. Takimiya, Y. Aso, T. Otsubo, M. Fujisuka, O. Ito, Org. Lett. 4 (2002) 309.
[50] O. Hagemann, M. Jorgensen, F.C. Krebs, J. Org. Chem. 71 (2006) 5546.
[51] (a) T. Nakamura, M. Fujisuka, Y. Araki, O. Ito, J. Ikemoto, K. Takimiya, Y. Aso, T. Otsubo, J. Phys. Chem. B 108 (2004) 10700;
(b) T. Nakamura, J-y. Ikemoto, M. Fujisuka, Y. Araki, O. Ito, K. Takimiya, Y. Aso, T. Otsubo, J. Phys. Chem. 109 (2005) 14365.
[52] M. Sun, P. Song, Y. Chen, F. Ma, Chem. Phys. Lett. 416 (2005) 94.
[53] X.X. Li, Y.-J. Guo, J.-W. Wang, L.-H. Kong, J.-H. Pan, Supramol. Chem. 20 (2008) 243.
[54] J. Rochford, A.D. Rooney, M.T. Pryce, Inorg. Chem. 46 (2007) 7247.
[55] T.B. Norsten, N.R. Branda, J. Am. Chem. Soc. 123 (2001) 1784.
[56] A. Liddell, G. Kodis, A.L. Moore, T.A. Moore, D. Gust, J. Am. Chem. Soc. 124 (2002) 7668.
[57] J.E. Park, E.J. Shin, Spectrochim. Acta Part A 68 (2007) 554.
[58] H.D. Samachetty, N.R. Branda, Chem. Commun. (2005) 2840.
[59] M. Yuasa, K. Oyaizu, A. Yamaguchi, M. Ishikawa, K. Eguchi, T. Kobayashi, Y. Toyoda, S. Tsutsui, Polym. Adv. Technol. 16 (2005) 287.
[60] K. Tammeveski, T.T. Tenno, A.A. Mashirin, E.W. Hillhouse, P. Manning, C.J. McNeil, Free Radic. Biol. Med. 25 (1998) 973.
[61] (a) F. Effenberger, H.C. Wolf, New J. Chem. 15 (1991) 117;
(b) F. Effenberger, H. Schlosser, P. Bauerle, S. Maier, H. Port, H.C. Wolf, Angew. Chem., Int. Ed. Engl. 27 (1988) 281;
(c) N. Holl, H. Port, H.C. Wolf, H. Strobel, F. Effenberger, Chem. Phys. 176 (1996) 215.
[62] J. Chen, A.K. Burrell, W.M. Cambell, D.L. Officer, C.O. Too, G.G. Wallace, Electrochim. Acta 49 (2004) 329.
[63] (a) R. Friedlein, F. Von Kieseritzky, S. Braun, C. Linde, W. Osikowicz, J. Hellberg, R. Salaneck, Chem. Commun. (2005) 1974;
(b) R. Friedlein, X. Crispin, W. Osikowicz, S. Braun, M.P. de Jong, C.D. Simpson, M.D. Watson, F. Von Kieseritzky, P. Samori, S.K.M. Jonsson, M. Fahlman, F. Jackel, J.P. Rabe, J. Hellberg, K. Mullen, W.R. Salaneck, Synth. Met. 147 (2004) 79.